Journal of Molecular Liquids 297 (2020) 111902

Contents lists available at ScienceDirect

Journal of Molecular Liquids

journal homepage: www.elsevier.com/locate/molliq

Silver clusters tune up electronic properties of graphene nanoflakes: A comprehensive theoretical study

Tabish Jadoon [a], Kevin Carter-Fenk [b], Muhammad Bilal Ahmed Siddique [c], John M. Herbert [b], Riaz Hussain [d], Sarosh Iqbal [c], Javed Iqbal [e,f], Khurshid Ayub [a,*]

[a] Department of Chemistry, COMSATS University Abbottabad Campus, 22060, Pakistan
[b] Department of Chemistry and Biochemistry, Ohio State University, Columbus, OH, 43210, USA
[c] Department of Applied Chemistry, Government College University, Faisalabad, Pakistan
[d] Department of Chemistry, University of Okara, Okara, Pakistan
[e] Department of Chemistry, University of Agriculture, Faisalabad, 38040, Pakistan
[f] Punjab Bio-energy Institute, University of Agriculture, Faisalabad, 38040, Pakistan

ARTICLE INFO

Article history:
Received 25 March 2019
Received in revised form 7 October 2019
Accepted 10 October 2019
Available online 23 October 2019

Keywords:
Silver-graphene composites
Surface interaction
Density functional theory
Electronic properties

ABSTRACT

Graphene-silver composites show a synergic effect of both components with enhanced electronic, adsorption and catalytic properties. We present here the detailed theoretical study on geometric, thermodynamic and electronic properties of silver clusters Ag_n (n = 2–10) adsorbed on graphene nanoflakes as a model for silver-graphene composites. First, a benchmark study is performed on Ag_n…coronene complexes (n = 2, 4) by evaluating various functional against reported high level ab-initio method for the selection of best functional for further calculations. Then, density functional theory study at the best chosen level is performed to inquire how clustering of adsorbate attached with carbon surface can impact geometric, electronic and thermodynamic properties of silver-graphene composites. Furthermore, the interaction energies are corrected for dispersion and basis set superposition error in order to get more realistic estimate of interaction energies. In progression, we investigated the dependence of interaction energy upon cluster size and dimensionality. For Ag_n…coronene, the binding energies increase monotonically as the number of atoms in the cluster increases. However, for Ag_n…dodecabenzocoronene, the interaction energies show a sudden drop at Ag_7…dodecabenzocoronene. The difference in behavior between Ag_n…dodecabenzocoronene and Ag_n…coronene for interaction energy is attributed to edge effect present in coronene. Furthermore, coplanar orientations of the silver clusters on polyaromatic hydrocarbons have higher interaction energies. The 2D-3D transition of the silver cluster is observed for Ag_7…coronene. CDA analysis reveals that backdonation from dodecabenzocoronene to silver clusters is more dominant in Ag_4–Ag_7 whereas other clusters have dominant charge transfer to dodecabenzocoronene. Charge transfer analysis via constrained density functional theory (CDFT) reveals significant energy lowering from charge donor-acceptor interactions. Further energy decomposition analysis (EDA) using absolutely-localized molecular orbitals (ALMO) suggests that, while charge-transfer is important in these systems, the sum of electrostatics, Pauli repulsion, and London dispersion are far more significant as silver cluster size increases. NCI results also support the presence of van der Waals and electrostatic interactions. The hollow top is most favorite interaction sites compared to bridge top and head top binding sites over coronene lattice. The ionization potential, electron affinity, frontier molecular orbital analysis, chemical hardness, softness, chemical potential, and Fermi levels are deliberated to verify the stability and reactivity of most stable silver-graphene composites. The remarkable outcome of the current findings makes our silver-graphene composite as a potential applicant for high performance electronic and catalytic devices.

1. Introduction

Graphene, a monolayer sheet of sp^2 hybridized carbon atoms [1], is the thinnest synthetic material which possesses certain unique properties due to its high surface area [2]. High thermal and electrical conductivity [3] of graphene combined with electronic [4], mechanical [5] and optical properties [6] have attracted many researchers to investigate its potential use in many applications [7–9]. Graphene-based materials are used as hydrogen storage devices [10], energy storage devices [11], electrodes [12], solid-state gas sensors [13], biosensors [14] and catalysts [15–17]. Pure graphene has zero band gap because valence

* Corresponding author.
E-mail address: Khurshid@cuiatd.edu.pk (K. Ayub).

https://doi.org/10.1016/j.molliq.2019.111902
0167-7322/

and conduction bands overlap at the Brillouin zone [18] which limits its use in various applications. This limitation is overcome by modifying the electronic structure of graphene through doping. The electronic properties and chemical reactivity of graphene are changed remarkably when graphene is doped with metal atoms or clusters [19]. Doping can be achieved either by replacing an atom of graphene with a dopant atom (substitutional doping) [20] or by placing a metal atom (or its cluster) on the surface of graphene [21]. The literature is quite rich for both types of doping of graphene. Wei Song et al. [22], evaluated the structural and electronic properties of Ni cluster doped graphene composites by using density functional theory. Metal doped (substitutional) graphene has been investigated both experimentally and theoretically for the adsorption of several gas molecules such as H_2, NO, NO_2, NH_3, CO, CO_2, H_2O_2 and TNT [19–29]. The results of these investigations prove that metal-doped graphenes are excellent candidates for gas sensors [30,31]. Besides the adsorption mechanism, oxidation and dissociation of molecules and also a catalytic mechanism of metal-doped graphene has been studied. Doping with transition metals is an excellent method to open the band gap and to provide an efficient way for electron transfer between transition metal and graphene. For surface doping of graphene, reports on metal clusters are more common than decoration with a single atom. Currently, the composite of graphene with the metal clusters of almost all transition metal are known to date [18–22]. Among these, the composites of graphene with late transition metals are of interest, more particularly of the coinage metals (Au, Ag & Cu) [32–36]. Many attempts have been made to form stable metallic clusters of groups IB (Au, Ag, Cu) of various sizes adsorbed on graphene. A DFT study has been carried out for aluminum doped graphene regarding its catalytic properties to be used for the conversion of methanol to gasoline [37]. Silver nanoparticles deposited graphene has been synthesized through the one-pot photochemical method and its high catalytic activity towards the reduction of 2-nitroaniline is investigated [38]. Thermal properties of silver nanoparticles-based graphene composites have also been experimentally studied. The applications of silver-based graphene composites in thermal management of advanced electronics and optoelectronics have been explored [39]. Liu et al. studied the electrical and optical properties of graphene silver nano-composites [40]. Duan Zhang and co-workers investigated the interaction mechanism of graphene and silver nanoparticles for the development of graphene-based electronic devices. It is notable that the surface enhanced Raman spectroscopy (SERS) is a powerful technique for identifying the number of graphene layers and investigating interaction mechanism [41]. The silver clusters are adsorbed on the surface of graphene by non-bonding interactions. Besides non-bonding complexes, composites involving covalent link between silver and graphene are also reported. Atomically precise clusters of silver covalently linked with graphene were synthesized and characterized by using UV–visible, luminescence, EDX, TEM, XPS and Raman spectroscopic techniques. These hybrid materials show the properties of both nanoscale materials. The results show that the hybrid material retains the spectroscopic characteristics of both the constituents and will be useful for vast applications in the areas of sensors, catalysis and drug delivery [42]. The growth of three-dimensional nanoparticles of silver on a few layers of graphene has been characterized by using scanning tunneling microscopy (STM) and with X-ray photoelectron spectroscopy.

DFT simulations were also used to determine the bonding, configuration, and energetics of interactions between small silver clusters (2, 4 atoms cluster) and graphene [43]. Granatier et al. investigated the interaction of graphene with dimer and tetramers of silver, gold, and palladium with MP2 and DFT methods. The validity of the MP2 calculations was confirmed for benzene-metal dimers complexes with benchmark values obtained at the CCSD(T) level. They have used a coronene molecule as a representative model for the graphene structure. It was found that silver and gold clusters bind with carbon surface through dispersion and charge transfer interactions whereas the palladium clusters bind with carbon surface through dative bonds. Calculations on coronene metal complexes at MP2 level indicated that the interaction energies of palladium, silver and gold tetramers are higher than the interaction energies of corresponding dimers. Among DFT methods, results at M06-2X methods are comparable to those from MP2 calculations. Moreover, the interaction energies of coronene metal complexes at M06-2X level are only slightly smaller than those in vacuum [44–47]. These investigations were also supported by the results of the stability of metal nanoparticles (~20 nm) on graphene composites [30–33] observed by scanning electron microscopy (SEM). In another combined experimental and theoretical report, Rao and coworkers studied the metal nanoparticle decorated graphene structures. They examined the interaction between graphene and metal nanoparticles of Ag, Au, Pt, and Pd by employing Raman spectroscopy and compared their results with theoretical calculations for M_{40} cluster on graphene. DFT study has been carried out for Pd_n clusters (n = 1–5) over graphene for the investigation of electronic properties [48]. Similarly, the interaction of graphene with other metals such as cobalt is also limited to only four atoms. The studies of Granatier and Rao are quite important regarding the interaction mechanism between the metal cluster and graphene, (although different models are used); however, they are limited to only 2, 4 or 40 atoms of the metal cluster on graphene. Some experimental and limited theoretical work on silver metal cluster decorated graphene composites are already reported in the literature [49–62]. The interaction energies, geometries and electronic properties of silver metal clusters on graphene surface are not known . With this motivation, we report here the detailed theoretical analysis of geometries, interaction energies and electronic properties of small silver clusters on coronene and dodecabenzocoronene, a model for graphene. This is the first study of its type where a complete range of silver cluster Ag_n (n = 2–10) is studied on the surface of coronene.

2. Computational methodology

Density functional theory (DFT) calculations were carried out with Gaussian 09 program package [63]. The interaction energies of silver tetramer on the surface of coronene are analyzed first with a variety of functional before concluding that M06-2X is the best functional for accurate determination of interaction energies. Then, M06-2X functional [47] with Los Alamos LANL2DZ effective core potentials were used for the optimization of the Ag_n...coronene (n = 2–10) system. The composites of silver with coronene are optimized with a variety of possible spin states (three lowest possible) to find correct spin multiplicity (SM) values for silver clusters-coronene surfaces. The spin multiplicity with the lowest energy was taken as the correct spin multiplicity for the system for further calculations. Vibrational frequency calculations were added in the equilibrium geometry calculations to check the stability of the obtained geometries and to obtain vibrational frequencies of the system. The following equation is used for the calculation of interaction energy.

$$BE = E_{Coronene---Ag_n\ adsorbed\ sytems} - (E_{Coronene} + E_{Metal\ Cluster}) \quad (1)$$

For Ag_n...dodecabenzocoronene (DBC), the geometries are taken from Ag_n...coronene complexes and the interaction energies are calculated at M06-2X/LANL2DZ. Furthermore, the interaction energies are corrected for dispersion and basis set superposition error. For dispersion correction, Grimme's D3 dispersion correction [64] is used with M06-2X method (M06-2X-D3). The Counterpoise method is used for the correction of basis set superposition error [65–67].

$$E_{int,CP} = E_{int} + E_{BSSE} \quad (2)$$

Electronic properties of Ag_n…coronene (n = 2–10) composites are calculated at M06-2X/LANL2DZ level of theory on the most stable spin state geometry. The frontier molecular orbital analysis (HOMO-LUMO) was conducted by full population analysis. After calculating the HOMO-LUMO gap, I.P and E.A were evaluated. The chemical hardness (η), softness (S) and chemical potential (μ) of silver metal clusters adsorbed on the surface of dodecabenzocoronene and coronene are calculated from VIP and EA by using the following equations (3)–(5) respectively.

$$\eta = \left(\frac{VIP-EA}{2}\right) \tag{3}$$

$$S = \left(\frac{1}{VIP-EA}\right) \tag{4}$$

$$\mu = -\left(\frac{VIP+EA}{2}\right) \tag{5}$$

where VIP is the vertical ionization potential and E.A is the electron affinity. The Fermi level of silver metal clusters adsorption on the surface of coronene is calculated by using the values of highest occupied molecular orbitals (HOMO) and lowest unoccupied molecular orbitals (LUMO) by using the following equation (6).

$$E_{FL} = \left(\frac{HOMO+LUMO}{2}\right) \tag{6}$$

Absolutely-localized molecular orbital energy decomposition analysis (ALMO-EDA) [68] was used to further separate the interaction energies in to components. The ALMO-EDA scheme decomposes the interaction energy into three contributions (equation (7)),

$$E_{int} = E_{FRZ} + E_{POL} + E_{CT}\ , \tag{7}$$

where E_{FRZ} is the frozen density energy, E_{POL} is electrostatic polarization, and E_{CT} is the energy lowering from charge donor-acceptor interactions. The frozen density energy encompasses the sum total of electrostatics, Pauli repulsion, and London dispersion contributions. There is some basis set dependence in the way that ALMO-EDA separates induced electrostatic interactions (polarization) from charge-transfer (CT), so a truncation of the polarization space at dipole and quadrupole response terms is enforced here via fragment electric-field response functions (FERFs).

An alternative definition of CT that is stable with respect to basis set and includes an infinite-order electrostatic polarization response is achieved with constrained density functional theory (CDFT) [69]. The CDFT method allows for real-space charge constraints via a Lagrangian formalism,

$$E_{CDFT} = E_{DFT} + \lambda\left(\int w_A(\boldsymbol{r})\rho(\boldsymbol{r})d\boldsymbol{r} - N_A\right)\ , \tag{8}$$

where N_A is the number of electrons on fragment A. In this work, the constraint is enforced using fragment-based Hirshfeld populations, where the weight function $w_A(\boldsymbol{r})$ is defined with respect to fragment indices as,

$$w_A(\boldsymbol{r}) = \frac{\rho_A(\boldsymbol{r})}{\sum_B \rho_B(\boldsymbol{r})}\ . \tag{9}$$

The CDFT CT energy is obtained after a second, canonical DFT calculation as the difference between the constrained and unconstrained DFT energies. All EDA/CT analyses were done using Q-Chem software package using the ω B97M − V functional [70] due to its excellent performance for non-covalent interaction energies [71].

3. Results and discussion

The literature reveals that M06-2X is a reliable DFT functional to deliver interaction energies for these clusters and the results are comparable to those obtained from high-level MP2 and CCSD (T) calculations. Close analysis of the results reveals that the interaction energies obtained with M06-2X are about 3–4 kcalmol^{-1} lower than those obtained from MP2 level calculations. Before proceeding further in our study, we considered a number of other DFT functional with two different low-cost basis sets for the interaction energy of Ag_4 with coronene. In the first approach, we have applied a mixed basis set where silver is treated with LANL2DZ pseudopotential and all carbon and hydrogen atoms are treated with 6-31G (d, p) Pople type basis set (Table 1). Unfortunately, the results with different functional for the interaction energies are worse than what is previously reported. The reported interaction energies at MP2/ANO-RCC-VDZ and M06-2X/LANL2DZ are −16.24 and −13.32 kcal mol^{-1} respectively, whereas the best value obtained in our hands was −13.04 kcalmol^{-1} for ωB97XD/6-31G (d, p). The interaction energy obtained with M06-2X was about −10.34 kcal mol^{-1}, which is about 3.0 kcal mol^{-1} less than the reported value at the same method but with a LANL2DZ basis set. After realizing that the mixed basis set approach is not very fruitful, the LANL2DZ basis set was applied for all atoms while using different functional. The value of interaction energy obtained here with M06-2X/LANL2DZ is −15.27 kcal mol^{-1}, this value is in fair agreement with reported −16.24 kcal mol^{-1} calculated at MP2/ANO-RCC-VDZ. This value is improved compared to the previously reported value of −13.04 kcal mol^{-1} at the same level. Since the M06-2X method gives superior results over other functional, energies of different orientations of Ag_4 on coronene were modeled and compared with the literature values. Hobza and co-workers have shown that Ag_4 can interact with the coronene in four possible ways. These four geometries include two different orientations of square Ag_4 and two for rhombic Ag_4. For the ease of calculations, we have performed calculations for rhombic Ag_4 on coronene and compared with the reported values by Hobza and co-workers. Surprisingly, the values in our hands were not only different than those reported earlier, but they were also better. The interaction energies obtained for these orientations are −15.17 and −15.18 kcal mol^{-1} compared to −13.68 and −13.32 kcal mol^{-1} in the literature. The interaction energies by us better correlate with the interaction energies of −16.49 and −16.24 kcal mol^{-1} obtained at MP2/ANO-RCC-VDZ. These findings are encouraging but confusing at the same time. It might be possible that these optimized structures are low energy minima compared to the previously reported geometries. In order to realize the spin contamination in these complexes, calculations have been performed with various multiplicities. The relative energies of the first higher spin multiplicities are shown in Table 2. Analysis of the results reveals that these complexes are more stable in the lowest spin state (singlet for even Ag clusters and doublet for an odd silver atom containing clusters). The relative energies of different spin states for a particular silver cluster do not follow any regular trend. For example, the singlet state for Ag_2…coronene is more stable than triplet state by −26.48 kcal mol^{-1}and this difference increases to −35.83 for Ag_3 but then, decrease to −8.15 kcal mol^{-1} for Ag_4 cluster. The highest difference of stabilities between multiplicities is observed for Ag_3…coronene (−35.83 kcal mol^{-1}) among all Ag_n (n = 2–10) clusters studied and the least difference is observed for Ag_6… coronene (−0.12 kcal mol^{-1}). The energy difference between different multiplicities for Ag_6…coronene is not significantly high, therefore, it can be expected that a higher spin structure may exist concomitantly. Furthermore, bonding of silver clusters at hollow top sites of coronene is preferred one compared with head top and bridge top sites Table 3.

Table 1
Interaction energy (E_b, in kcal mol^{-1}) of rhombic-Ag_4 (rh–Ag_4) clusters over coronene substrate calculated at different methods with pure basis set (LANL2DZ) and mixed basis set (6-31G (d,p) & LANL2DZ).

Functional	B3LYP	LSDA	B3PW91	PBEPBE	MPWPW91	M05-2X	M06-2X	ωB97XD	B3LYP-D3
Interaction Energies[a]	−0.06	−26.82	−8.16	−12.21	−4.34	−14.92	−15.27	−19.69	−21.92
Interaction Energies[b]	2.63	20.71	−0.18	−0.85	0.35	−5.73	−10.34	−13.05	−12.38

a Interaction Energies @ **LANL2DZ**.

b Interaction Energies @ **6−31G (d,p) & LANL2DZ)**

Table 2
Electronic energies (a.u), Interaction energies (kcal mol^{-1}) and Relative energies (eV) at various spin states for most stable Ag_n…coronene (n = 2–10) composites at M06-2X/LANL2DZ.

	Multiplicities	Electronic energies	Interaction energies	Relative energies
Ag_2…	Singlet	−1212.80	−8.87	0.00
coronene	Triplet	−1212.75	–	1.148
Ag_3…	Doublet	−1358.49	−13.18	0.00
coronene	Quintet	−1358.43	–	1.553
Ag_4…	Singlet	−1504.20	−15.28	0.00
coronene	Triplet	−1504.19	–	0.353
Ag_5…	Doublet	−1649.91	−18.57	0.00
coronene	Quintet	−1649.88	–	0.941
Ag_6…	Singlet	−1795.64	−23.26	0.00
coronene	Triplet	−1795.64	–	0.005
Ag_7…	Doublet	−1941.34	−24.21	0.00
coronene	Quintet	−1941.31	–	0.949
Ag_8…	Singlet	−2087.07	−25.09	0.00
coronene	Triplet	−2087.04	–	0.805
Ag_9…	Doublet	−2232.77	−29.30	0.00
coronene	Quintet	−2232.74	–	0.808
Ag_{10}…	Singlet	−2378.49	−30.60	0.00
coronene	Triplet	−2378.47	–	0.399

3.1. Energies and geometries of Ag_n…coronene (n = 2–10) composites

Theoretical investigation on adsorption energy and geometry of silver dimer (Ag_2) on graphene was carried out by using density functional theory (DFT). Since the geometries of Ag_2…coronene and Ag_4…coronene are already discussed in the literature, therefore, a discussion on their geometries will be very limited in this manuscript. We will describe only the energy difference that we observed from the literature values. It is worth mentioning here that first the silver clusters with a smaller coronene model are studied to get an idea about the relative stabilities of different clusters. The lowest energy structures obtained from silver coronene model are then taken for the optimization of silver-dodecabenzocoronene (DBC), a bigger model.

3.1.1. Ag_2…coronene

Ag_2 dimer can be placed on coronene in two different orientations i.e., parallel to the plane of coronene (∥-Ag_2…coronene) or perpendicular (⊥-Ag_2…coronene) to the plane of coronene. Hobza and co-workers have considered only parallel orientation and various different geometries are obtained for Ag_2 dimer parallel to coronene. However, in this work, we have considered the perpendicular orientation as well. Surprisingly, the perpendicular orientation of Ag_2 on coronene is more stable than the parallel orientation. The Ag_2…coronene with perpendicular orientation (⊥-Ag_2…coronene) has the highest stability (global minimum) and the interaction energy is −8.87 kcal mol^{-1} (Fig. 1). In this structure, the Ag_2 does not reside perpendicular to the central ring, rather it is interacting with only one carbon atom of the central carbon. The distance of the silver atom of the perpendicular dimer on coronene is 2.79 Å (Fig. 2). A number of other orientations are also possible where the perpendicular dimer can interact with the carbons of the peripheral ring, but those orientations are not considered here because those positions bear hydrogen atoms and do not represent a model graphene structure except edges of graphene. For the parallel orientations, quite similar to the reported literature, we could find a number of orientations with comparable energies. The lowest energy structure is the one where silver dimer resides perpendicular to the central carbon ring and the distance of Ag_2 from the coronene ring is 3.27 Å, and the interaction energy is −8.30 kcal mol^{-1}.

Table 3
Adsorption energies, the bond distance of Ag–Ag, and Ag … X from the various adsorption sites of Ag_n…coronene (n = 2–10) composites at M06-2X/LANL2DZ. Symbol **⊥, ∥, ↑ & ↓** represent perpendicular, parallel, up & down orientation respectively.

Ag_n … coronene	d $_{Agn\ \ldots\ X}$			d $_{Ag-Ag}$	E_{int} (kcal mol^{-1})
	d $_{C-Ag}$	d $_{b\text{-}Ag}$	d $_{h\text{-}Ag}$		
Ag_2∥… X	3.27 (2)	–	–	3.27	−8.30
Ag_2 ⊥ … X	2.79 (1)	–	–	2.68	−8.87
a-Ag_3… X	–	–	3.02 (3)	2.78	−13.18
b-Ag_3… X	2.83 (1)	–	–	2.75	−8.533
rh-Ag_4⊥ … X	2.70 (1)	3.40 (2)	4.72 (1)	2.90	−15.22
rh-Ag_4∥… X	3.1 (2)	–	3.39 (2)	2.96	−15.28
Y –Ag_4∥… X	–	3.45 (1)	3.34 (3)	2.86	−15.45
Y –Ag_4⊥ … X	3.10 (2)	–	–	2.86	−11.53
W–Ag_5∥… X	3.44 (1)	3.37 (1)	3.30 (3)	2.97	−18.57
W–Ag_5(↑)… X	–	3.24 (2)	3.18 (1)	2.90	−13.84
W–Ag_5(↓)… X	2.97 (1)	–	3.32 (1)	2.91	−11.99
a-Ag_6… X	–	–	3.25 (6)	2.94	−21.45
b-Ag_6… X	2.78 (1)	–	–	2.95	−17.30
c-Ag_6… X	–	–	3.36 (2)	3.08	−19.37
d-Ag_6… X	–	3.13 (1)	3.12 (2)	2.93	−23.26
a-Ag_7… X	3.41 (1)	–	–	3.02	−16.14
b-Ag_7… X	–	–	3.38 (7)	2.96	−24.21
a-Ag_8… X	–	–	3.51 (8)	2.94	−25.09
b-Ag_8… X	–	–	3.07 (3)	2.94	−15.91
c-Ag_8… X	–	–	3.01 (3)	2.99	−16.37
d-Ag_8… X	3.23 (1)	… … …	3.18 (3)	2.97	−17.53
a-Ag_9… X	3.12 (1)	3.18 (2)	3.60 (3)	2.97	−29.29
b-Ag_9… X	–	–	3.30 (7)	2.92	−18.22
c-Ag_9… X	6.0 (1)	5.89 (2)	3.30 (5)	3.05	−19.83
d-Ag_9… X	3.03 (3)	3.12 (2)	3.42 (4)	2.93	−16.14
e-Ag_9… X	3.35 (1)	3.38 (3)	3.32 (3)	2.94	−26.29
a-Ag_{10}… X	5.52 (2)	–	3.02 (5)	2.94	−30.60
b-Ag_{10}… X	–	6.0 (1)	3.20 (7)	2.93	−28.83

3.1.2. Ag_3…coronene

For Ag_3…coronene complex, the complexity increases many folds, not because of the several orientations possible for Ag_3 on coronene but also due to the existence of Ag_3 in various shapes. For example, silver trimer can exist in two geometries, although not differing much in energy and structure. Previously, we had shown by calculations at TPSSTPSS method that a slightly bent structure is marginally stable than a perfectly linear Ag_3 by 0.35 kcal mol^{-1}. For Ag_3…coronene complex, several different geometries are optimized, and their interaction energies are calculated. It is worth mentioning that for the calculation of interaction energies, the energies of corresponding silver trimer are taken. For example, for linear Ag_3 optimized on coronene, the energies of linear Ag_3 and coronene are taken. For silver trimer, the linear Ag_3 … coronene complex is more stable for perpendicular geometry of Ag_3 whereas the obtuse triangle structure is more stable for parallel orientation of Ag_3 on coronene. Among these two complexes, obtuse triangle (C_{2v} symmetry) Ag_3…coronene complex is the low energy structure compared to the linear Ag_3…coronene complex by 4.39 kcal mol^{-1}. The interaction energies of linear and obtuse Ag_3 on the surface of coronene are −8.60 and −13.18 kcal mol^{-1}, respectively. Linear Ag_3 is present perpendicular to the coronene at a distance of 2.83 Å (b-Ag_3…coronene, Fig. 2). Further, it is found that there is a change in bond angle in the case of angular silver trimer over coronene from 153° to 146°. The obtuse triangle Ag_3 is found at a distance of 3.02 Å over the coronene, in which each atom of the silver trimer is present at the hollow site of three benzene rings of coronene (a-Ag_3…coronene, Fig. 2). The discussion here and in the subsequent sections is limited to only those structures where Ag clusters are optimized with central orientation on the coronene ring.

3.1.3. Ag_4…coronene

The geometries of Ag_4….coronene complexes are already discussed in the literature; however, the discussion was limited to the only planar orientation of Ag_4 on the coronene ring (see Fig. 2).

Quite similar to Ag_2…coronene complex, the perpendicular orientations of Ag_4 on the coronene are also studied. Quite contrary to Ag_2…coronene complex, perpendicular orientation of Ag_4 on coronene (∥-Ag_4…coronene) is not the most stable. Among all attempted structures, four distinct structures optimized were; rhombic Ag_4 perpendicular to coronene (rh-Ag_4-⊥…coronene), rhombic Ag_4 parallel to coronene (rh-Ag_4-∥…coronene), Y shaped Ag_4 parallel to coronene (Y–Ag_4-∥…coronene), and Y shaped Ag_4 perpendicular to coronene (Y–Ag_4-⊥…coronene). The relative energies of these geometries are 0, 0.26, 3.10 and 7.02 kcal mol^{-1} for rh-Ag_4-∥…coronene, rh-Ag_4-⊥…coronene, Y–Ag_4-∥… coronene and Y–Ag_4-⊥…coronene, respectively. Pure Ag_4 also exists in distorted tetrahedron geometry however, all attempts to optimize its complex with coronene converged to rh-Ag_4…coronene geometry. Quite similar to other Ag_n complexes, Ag_4 coronene

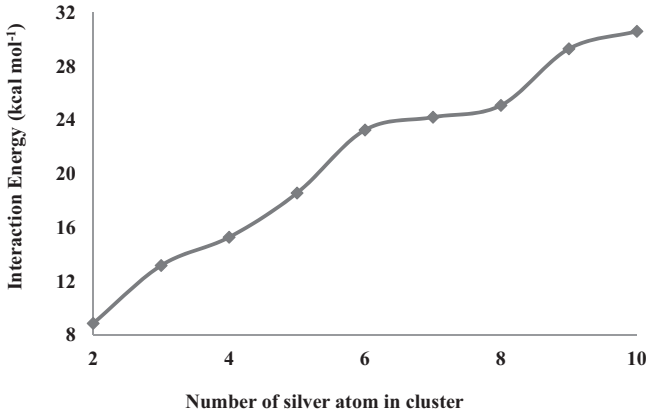

Fig. 1. Interaction energy (kcal mol^{-1}) of most stable Ag_n…coronene (n = 2–10) composites.

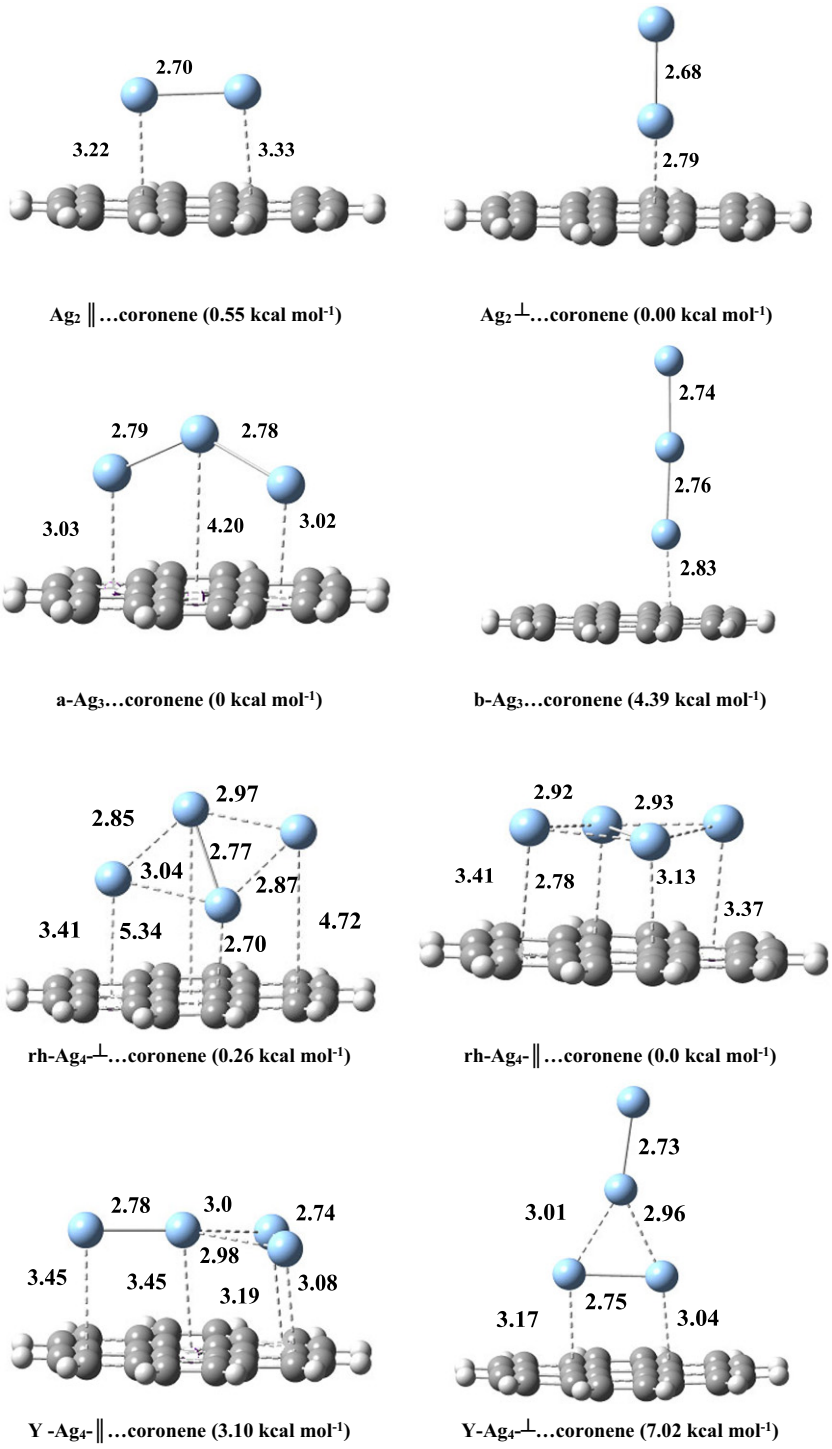

Fig. 2. Side view of Ag_2…coronene, Ag_3…coronene and Ag_4…coronene composites. Values shown in parantheiss are relative energies in kcal mol^{-1} whereas the bond distances shown in figure are in Angstroms.

complex is also optimized in various close-lying structures for each rhombus or Y-shaped clusters. However, their energies are so close that they are not worth discussing in the manuscript. Their structures and energies are given in the supporting information. In terms of interaction energies, Y–Ag_4-‖…coronene has the highest interaction energy of −15.50 kcal mol^{-1}. The interaction energies of Ag_n clusters on coronene increases with an increase in the size of the silver cluster. The interaction energy of the Ag_4 cluster is about 2.10 kcal mol^{-1} higher than that for Ag_3…coronene. The higher interaction energy arises from the higher number of interactions in Ag_4 compared to Ag_3 with coronene. In Ag_3 only two terminal atoms are interacting with the coronene ring whereas, in Ag_4, all silver atoms interact with the coronene ring. However, a detailed discussion on the involvement of charges on each silver atom in these clusters is beyond the scope of the current study.

3.1.4. Ag_5…coronene

Different structures of silver pentamer (Ag_5) on coronene are optimized in order to evaluate the interaction behavior with coronene (see Fig. 3). Pure Ag_5 is optimized in three distinct geometries namely W-shaped, square planar and envelope shape; however, during optimization on coronene, all these silver cluster structures changed to W-shaped. The silver cluster in W-shape on coronene can also attain different orientations of a silver cluster. The orientation where Ag_5 cluster is parallel to the plane of coronene is more stable than the perpendicular orientation. For the planar orientation of the W-shaped cluster on coronene, three different geometries were optimized. One of them is presented here whereas the remaining two structures are shown in the supporting information. The two optimized structure differ only in the position of silver atom on the coronene skeleton. The interaction energies for Ag_5 on coronene in parallel orientation range from −18.41 to

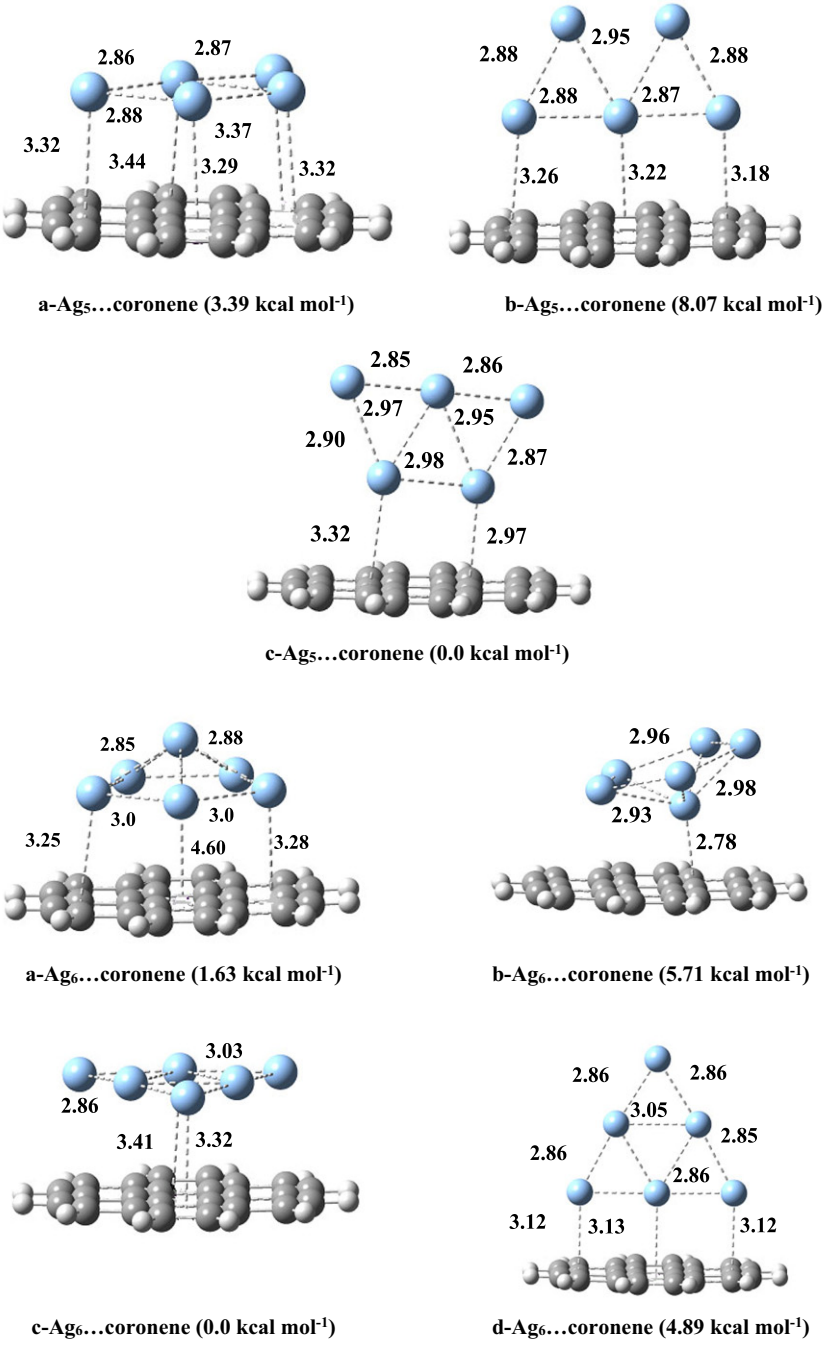

Fig. 3. Side view of Ag_5…coronene and Ag_6…coronene composites. Values shown in parantheiss are relative energies in kcal mol^{-1} whereas the bond distances shown in figure are in Angstroms.

−18.57 kcal mol^{-1}. The interaction energies of Ag_5 on coronene are about 3 kcal mol^{-1} higher than those for Ag_4. The average Ag…coronene distance in the most stable structure (a-Ag_5…coronene) is 3.3 Å and each silver atom is present at the hollow top sites of coronene (Table 3). For the perpendicular orientation of W-shaped Ag_5 on coronene, two orientations are observed namely W 'up' (b-Ag_5…coronene) & W 'down' (c-Ag_5… coronene). The W 'up' structure is higher in energy than the W 'down' structure. The former has the interaction energy of −12.12 kcal mol^{-1} whereas the latter has the interaction energy −13.90 kcal mol^{-1}. The inter planer distance in case of W 'down' structure from coronene is 3.22 Å whereas W 'down' structure is slightly inclined on coronene. The lower-lying silver atom of W 'up' structure from the surface of coronene is located at a distance of 2.97 Å.

3.1.5. Ag_6…coronene

Interaction mechanism of four different Ag_6 silver cluster with coronene is studied, and it is observed that the Ag_6 cluster on coronene in the optimized structure exists in two geometries; pentagon pyramid or planar triangular with an atom in the center of each side (see Fig. 3). Since other input geometries of Ag_6 changed to one of the above-mentioned geometries therefore, those are not discussed here separately. Pentagon pyramid on coronene is located parallel to the coronene plane with pyramid up (a-Ag_6… coronene) or pyramid down (b-Ag_6…coronene). For pyramid up orientation (a-Ag_6… coronene), five atoms of pentagon pyramid interact at a distance of 3.26 Å with the rings of the coronene whereas the sixth atom is located at a slightly large distance of 4.61 Å. The pyramid down Ag_6 (b-Ag_6…coronene) interacts less favorably with coronene compared to the pyramid up (vide infra). The interaction energy of Ag_6 in the pyramid down structure is −17.42 kcal mol^{-1} compared to −21.47 kcal mol^{-1} for pyramid up orientation.

All the distances are in Å, the lowest values of bond distance in all cases of Ag_n…X, while for Ag–Ag average distance is taken. The adsorption energies (Ea) are in eV, n is the number of atoms of the silver clusters, and X represents the coronene substrate. The d_{C-Ag}, d_{b-Ag}, and d_{h-Ag} represents the head top, bridge top and hollow top bonding sites, respectively. The number of binding sites is presented in parenthesis.

For planar orientation, quite similar to the above discussed clusters, various geometries with close energies are observed (see supporting information). The pentagonal pyramid pure Ag_6 is less stable than planar triangular Ag_6 by 3.86 kcal mol^{-1}. However, this

difference is decreased for their coronene complexes which indicate the higher binding energy of pentagon pyramid Ag_6 with coronene. The interaction energy of pentagon pyramid Ag_6 with coronene is −21.48 kcal mol^{-1} (a-Ag_6…coronene), compared to −19.39 kcal mol^{-1} for planar triangular Ag_6…coronene (c-Ag_6…coronene). Despite the higher interaction energies of pentagon pyramid Ag_6…coronene complexes, these coronene complexes are about 1.63 kcal mol^{-1} less stable than planar triangular Ag_6 complex (c-Ag_6…coronene) mainly due to the intrinsic instability of the precursor pure Ag_6 cluster. For c-Ag_6…coronene and a-Ag_6…coronene, the Ag_6 clusters are at distances of 3.33 Å and 3.26 Å, respectively from the surface of coronene. As shown the perfectly planar Ag_6 is also optimized in a perpendicular orientation where 3 atoms of Ag_6 interact with the coronene ring at 3.12 Å (d-Ag_6…coronene. The interaction energy for this d-Ag_6…coronene is −14.35 kcal mol^{-1}, about 5 kcal mol lower than the coplanar structures. The Ag_6…coronene has extra stability than Ag_5…coronene system in terms of the more interaction energy of 2.91 kcal mol^{-1}.

3.1.6. Ag_7…coronene

From the analysis of the results above, the planar structures are more stable than their non-planar analogues on the surface of coronene which is attributed to the increased number of interactions in planar geometries. Therefore, for Ag_7, only two structures are considered for adsorption on coronene; heptagonal planar and pentagonal bipyramidal. It is interesting to note that these silver clusters did not change their geometries during optimization. For distorted pentagonal bipyramidal Ag_7, a-Ag_7…coronene is the most stable structure although this structure is not the one with the highest interaction energies among all Ag_7…coronene structures. The distorted pentagonal bipyramidal Ag_7 is more stable than planer hexagon Ag_7 by an amount of 5.30 kcal mol^{-1}. Planar hexagon orientation of Ag_7…coronene (d- Ag_7…coronene) is the most stable geometry regarding the interaction energies (E_{int} = −24.21 kcal mol^{-1}). Moreover, in the case of d-Ag_7… coronene, all the silver atoms are present at hollow sites on coronene (top view). The Ag_7…coronene system is more stable than Ag_6…coronene system by 2.73 kcal mol^{-1}.

3.1.7. Ag_8…coronene to Ag_{10}…coronene

The interaction mechanism of two different structures of Ag_8…coronene system is investigated. Two different low energy structures of Ag_8 were considered here; planar and non-planar. For Ag_8, the non-planar structure is more stable than the planar one however; the interaction energies are higher for planar Ag_8 on coronene. Planar Ag_8 in parallel orientation with coronene (a-Ag_8…coronene) has the highest interaction energy of −25.10 kcal mol^{-1} whereas in case of the perpendicular orientation of this Ag_8 on coronene (b-Ag_8…coronene) has merely −16.05 kcal mol^{-1} interaction energy. The interaction energy of non-planar Ag_8 on coronene (c-Ag_8…coronene) is-17.51 kcal mol^{-1}.

The c-Ag_8…coronene changed its structure on coronene during optimization. The resulting geometry has 3 silver atoms interacting with coronene followed by another lay of four silver atoms. The last Ag atom is present at the apex. However, the d-Ag_8… coronene in which Ag_8 did not change its geometry on coronene has a slightly lower interaction energy of −16.38 kcal mol^{-1}. Despite a-Ag_8…coronene has the highest interaction energy but yet, it is not the lowest energy structure. The most stable structure in terms of total electronic energy is c-Ag_8…coronene, see Fig. 4 for details. The c-Ag_8…coronene is more stable than a-Ag_8…coronene by an amount of 11.03 kcal mol^{-1}. For a-Ag_8… coronene, where all silver atoms are present in one plane has interplaner distance of 3.38 Å from coronene compared with 3.13 Å in case of c-Ag_8…coronene, where three silver atoms are in a lower-lying plane. The Ag_8…coronene system is more stable by an amount of 0.87 kcal mol^{-1} than Ag_7…coronene system. In the case of silver nonamer, five different structures are studied to get information about the interaction mechanism with coronene. The a-Ag_9…coronene has interaction energy of −29.30 kcal mol^{-1}and it is more stable than b-Ag_9…coronene by an amount of 9.63 kcal mol^{-1}. However, their difference in interaction energies is only 2.45 kcal mol^{-1} (compare 29.30 for a-Ag_9…

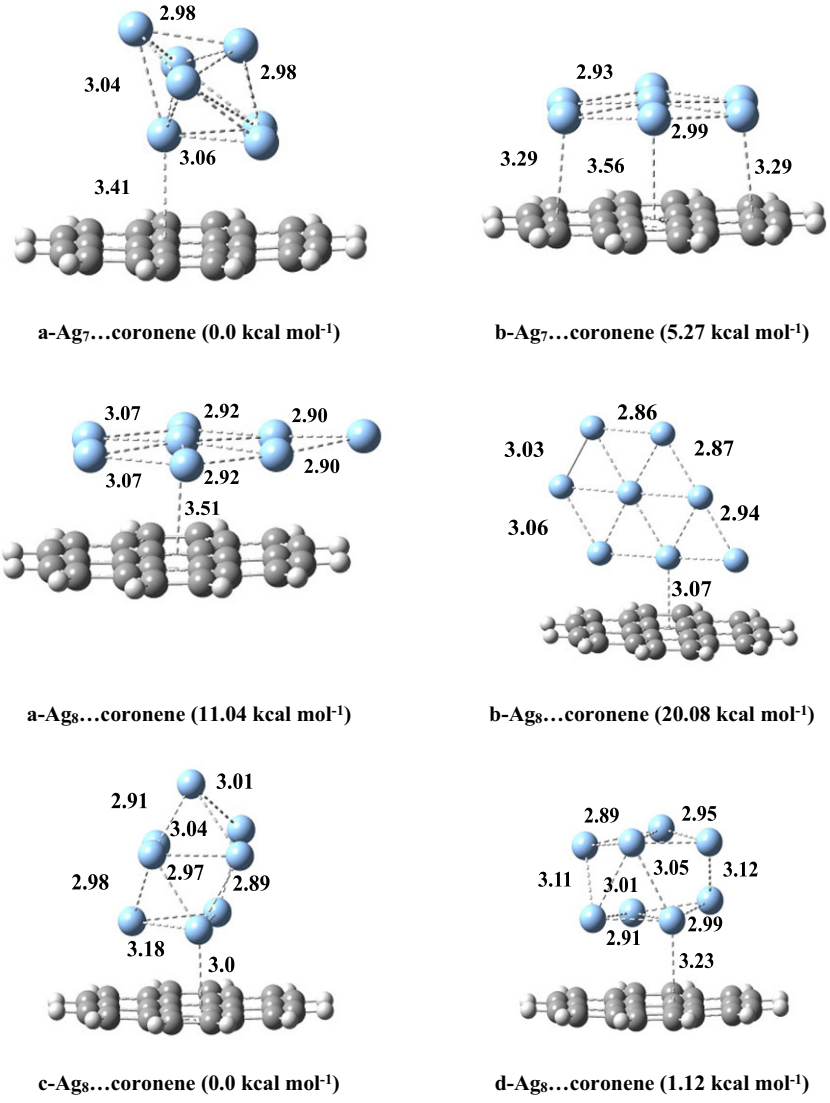

Fig. 4. Side view of Ag_7…coronene and Ag_8…coronene composites. Values shown in parantheiss are relative energies in kcal mol^{-1} whereas the bond distances shown in figure are in Angstroms.

coronene to 26.84 kcal mol^{-1} for b-Ag$_9$…coronene). It is also observed that c-Ag$_9$…coronene is more stable than d-Ag$_9$…coronene, e-Ag$_9$…coronene, b-Ag$_9$…coronene, and a-Ag$_9$…coronene by 4.76, 9.72, 11.7 and 2.07 kcal mol^{-1} respectively (Fig. 5).

In terms of the interaction energy of the overall Ag$_9$…coronene system, the a-Ag$_9$…coronene is more stable than c-Ag$_9$…coronene, d-Ag$_9$…coronene, e-Ag$_9$…coronene, and b-Ag$_9$…coronene by 9.44, 13.09, 2.95 and 2.45 kcal mol^{-1} respectively. In case of a-Ag$_9$…coronene, the two lower-lying silver atoms of Ag$_9$ are found at inter planer distance of 3.05 Å over the coronene ring. The Ag$_9$…coronene system is more stable than Ag$_8$…coronene system by 4.21 kcal mol^{-1}.

The interaction of Ag$_{10}$ with coronene is investigated and it is found that a-Ag$_{10}$…coronene has interaction energy of −30.60 kcal mol^{-1}. The inter planer distance between two low lying silver atoms of Ag$_{10}$ cluster from coronene ring is 2.96 Å. The interaction energy of b-Ag$_{10}$…coronene is −28.86 kcal mol^{-1}, and for the value of interaction energy in case of a-Ag$_{10}$…coronene, is the higher than the interaction energies of all silver clusters coronene system studied. The interaction energy of Ag$_{10}$…coronene system is more than Ag$_9$…coronene system by an amount of 1.29 kcal mol^{-1}. In this orientation, the three lower-lying silver atoms are found at 3.20 Å from the coronene ring.

Coronene is a smaller model for graphene regarding interaction energies with silver clusters. It is expected that with increase in the size of the cluster, chances of silver atoms with edges of coronene increases. The edges can cause unusual increase in the interaction energies due to edge effect. Therefore, we have optimized silver clusters on dodecabenzocoronene (DBC) in order to eliminate edge effect. The interaction mechanism of silver cluster decorated dodecabenzocoronene is investigated with M062X method of DFT. The most stable orientation of Ag^n on coronene are taken as model for Ag$_n$…DBC complexes. Silver cluster binds with carbon surface through dispersion interaction and to get a clear idea about the nature of interaction dispersion correction DFT-D3 is included. It is well recognized that dispersion energy is an important component of overall stabilization energy in silver graphene composites which are held together by dispersion

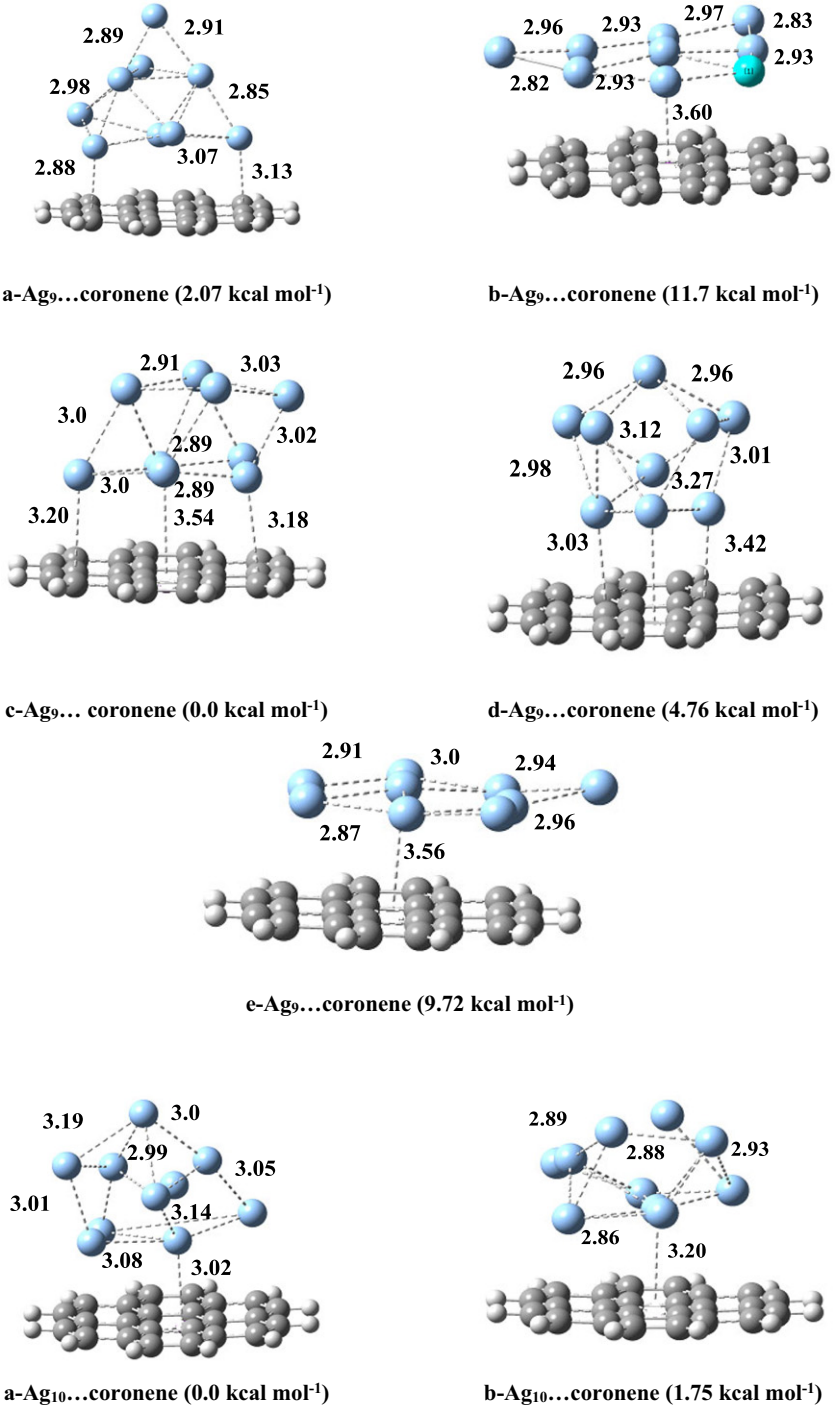

Fig. 5. Side view of Ag$_9$…coronene and Ag$_{10}$…coronene composites. Values shown in parantheiss are relative energies in kcal mol^{-1} whereas the bond distances shown in figure are in Angstroms.

interactions. The stronger dispersions interactions between silver graphene composites are due to greater polarizability of silver metal. It can be seen from the results of interaction investigation that the interaction energy increases with the number of silver atoms interacting with dodecabenzocoronene ring. Although a similar trend of interaction energies is found for both M062X and M062X-D3 methods, the interactions are more prominent in the case of M062X-D3 (see Fig. 6).

The results of interaction energies calculated at M062X-D3 reveal that the interaction energies of Ag_2, Ag_3, Ag_4, Ag_5 & Ag_6 are −13.88, −19.33, −22.01, −27.12 and −30.23 kcal mol^{-1}, respectively (Table 4). The stability of silver clusters increases regularly up to hexamer due to their planer orientation which provides larger interacting surface between the silver cluster and DBC ring. The interaction energies depend on the number of silver atoms in cluster interacting with carbon surface of DBC ring and on the nature of interaction sites such as head top, hollow top and bridge top. The interaction energy then suddenly fall out in cases from heptamer to nonamer silver cluster adsorption over the DBC surface. The decrease in interaction energies is due to the smaller number of silver atoms present in the lower-lying plane of a cluster that interacts directly with DBC ring. The interaction energies for Ag_7…DBC, Ag_8…DBC & Ag_9…DBC composites are 24.75, 25.37 & 29.60 kcal mol^{-1} with minimum C···H distances of 3.25, 3.05 & 3.27 Å, respectively. Moreover, the interaction energies of Ag_8…DBC & Ag_9…DBC are also smaller than Ag_6…DBC which strongly suggests that the edge effect was strongly prevailing in the corresponding coronene complexes. The heptamer, octamer & nonamer silver cluster decorated DBC composites are relatively more stable than dimer silver cluster by an amount of interaction energies of 10.87,11.49 & 15.72 kcal mol^{-1}, respectively. The decamer silver cluster (see Fig. 7) show the highest stability amongst all studied Ag_n (n = 2–10) silver clusters. The interaction energy of Ag_{10}…DBC composite is 41.03 kcal mol^{-1}. The decamer silver cluster decorated DBC composites show the highest stability and it has 27.15 kcal mol^{-1} more interaction energy than silver dimer decorated DBC composite. The minimum C···H distance of 3.13 Å is found in case of decamer silver cluster adsorption over DBC surface. The higher interaction energy in case of silver cluster decorated DBC composites is due to possible overlapping effect between d & π-states of silver and DBC ring in addition to long-range dispersive interactions.

The interaction energies calculated at M06-2X-D3 are corrected for basis set superposition error. The BSSE corrected energies follow the same trend, as observed for M06-2X-D3. The BSSE correction is typically about 10–15% of the dispersion corrected energies. The highest BSSE correction in terms of percentages is seen for Ag_9…DBC where BSSE correction is about 15.2% of the interaction energy. The highest BSSE correction in terms of kcal mol^{-1} is seen for Ag_{10}…DBC where BSSE correction is 4.76 kcal mol^{-1}.

3.2. Non-covalent interaction (NCI) index analysis

NCI (Non-Covalent Interactions) is a technique which is based on the density and its derivatives. NCI is extensively used currently to get understandings about non-covalent interactions such as van der Waals interactions, hydrogen bonds, and steric clashes. NCI is a dynamic technique for the identification and classification of the noncovalent interactions in complexes based on the RDG (reduce density gradient). The RDG is calculated by taking the first derivative of electron density ρ(r) by the following formula.

$$RDG = \frac{1}{2(3\pi^2)^{1/3}} \frac{|\nabla\rho(r)|}{\rho(r)^{4/3}}$$

where ρ and ∇ρ are denoted to as electronic density and electronic density gradient, respectively. The RDG is a dimensionless function which is used to define the departure from homogenous electron distribution. The reduced gradient has very large positive

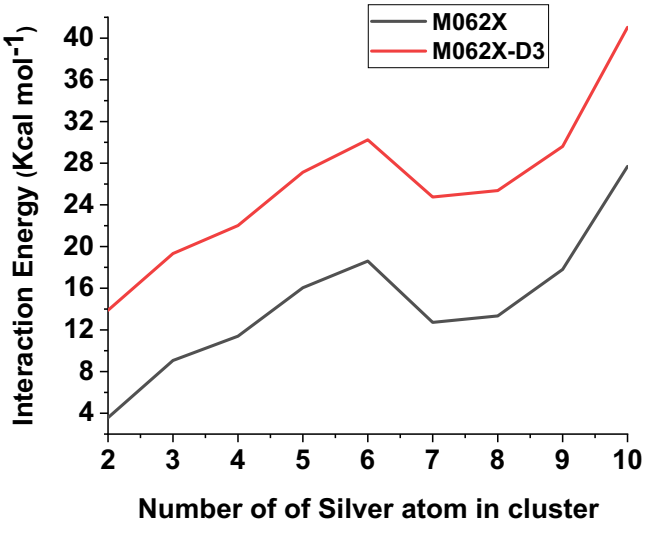

Fig. 6. Interaction Energy of most stable Ag_n… DBC (n = 2–10) composites.

Table 4
Interaction energies of **Ag_n… DBC** complexes calculated at M06-2X, M06-2X-D3 and M06-2X-D3 with basis set superposition error correction, while using LANL2DZ basis set.

Ag_n … DBC composite	Interaction energy at M06-2X (kcal mol^{-1})	Interaction energy at M06-2X-D3 (kcal mol^{-1})	Interaction energy at M06-2X-D3 with BSSE correction (kcal mol^{-1})
Ag_2…DBC	−3.56	−13.88	−12.31
Ag_3…DBC	−9.06	−19.33	−16.64
Ag_4…DBC	−11.39	−22.01	−18.88
Ag_5…DBC	−16.05	−27.12	−23.36
Ag_6…DBC	−18.60	−30.23	−26.02
Ag_7…DBC	−12.71	−24.75	−21.26
Ag_8…DBC	−13.33	−25.37	−21.82
Ag_9…DBC	−17.80	−29.60	−25.10
Ag_{10}…DBC	−27.69	−41.03	−36.27

value far from the molecule because at that point electronic density dies off exponentially to zero. In the region of covalent and non-covalent interactions, the RDG has very small values (close to zero). The noncovalent interactions are explained satisfactorily through NCI index analysis. The colored iso-surfaces are obtained on RDG iso-surfaces by mapping sign (λ_2) ρ(r). Literature tells that the RDG iso-surface is based on a color scheme as a code: red-yellow-green-blue. Where red color indicates the steric repulsion, the blue color represents the non-covalent attractive forces while green and yellow color characterizes weak attractive and repulsive forces. To determine the type of interactions, three eigenvalues (λ_i) of Hessian, the second derivative of electron density are calculated ($\lambda_1 \le \lambda_2 \le \lambda_3$). At nuclei (the density is at local maximum) all the eigenvalues are negative. For covalent interactions, two of the eigenvalues of Hessian are negative while the third one is positive. On the other hand, in the region of steric clashes, the second eigenvalue is positive, and this value is used to distinguish between covalent and non-covalent interactions. The eigenvalue is negative ($\lambda_2 < 0$) for covalent and non-covalent interactions, while it is positive ($\lambda_2 > 0$) for destabilizing repulsive interactions. The strength of non-covalent interactions is directly related to density. The stronger interactions are indicated by higher density values while weaker interactions through lower density value.

NCI plot with iso-surface visualization for the most stable silver cluster decorated DBC ring is given in Fig. 8. (The rest of the NCI plot with iso-surface visualization are given in Fig. N1–N8 of supporting information). The shifting of spike either toward negative or positive $\lambda_2\rho$ by the interactions of the silver cluster with DBC surface clearly demonstrates the nature of interactions.

The RDG study reveals that silver cluster decorated DBC composites are stabilized by Ag…C (d-π) electrostatic interactions, as well as van der Waals interaction (dispersion). For Ag_2…DBC composite, the scatter maps indicate that there exist three spikes, at the bottom the negative region of $\lambda_2\rho$ (−0.04 a. u) indicates the electrostatic interactions. The low gradient peak which appears at the positive side (+0.02 a. u), indicate the existance of steric repulsion. The red peak denotes the depletion of electron density due to electrostatic repulsion. There is not much significant green RGD isosurface ($\lambda_2\rho = 0$ a. u), which should be considered that there are negligibly weak van der Waals dispersion interactions. In addition, blue-green disc-like NCI isosurface is observed between the silver cluster and DBC ring which also indicates weak van der Waals interactions. The RGD isosurface map for Ag_3…DBC & Ag_4…DBC indicate that gradient peaks appear at the negative region with almost similar $\lambda_2\rho$ values (−0.03 a. u), that accounts for electrostatic interactions. The green peak appears at $\lambda_2\rho = -0.01$ a. u, for both composites which suggest van der Waals dispersive interactions. The red peak associated with steric repulsion appears at $\lambda_2\rho = 0.02$ a. u for both trimer and tetramer silver cluster decorated DBC composite. In the case of Ag_5…DBC & Ag_6…DBC, the peaks related to strong electrostatic interactions originate at $\lambda_2\rho = -0.03$ to −0.02 a. u. The peaks appear at $\lambda_2\rho = -0.01$ & $\lambda_2\rho = +0.02$ corresponds to dispersion interactions and steric clashes, respectively. In the case of Ag_7…DBC, all three peaks have appeared almost at $\lambda_2\rho = -0.02$, −0.01 & +0.02 a. u, which indicate that electrostatic & dispersive interactions along with steric repulsions are there in the composite. In Ag_8…DBC composite, the blue, green and red spikes appear at $\lambda_2\rho = -0.04$, −0.1 & 0.04 a. u, respectively but these are not much sharper at the bottom. In the case of Ag_9…DBC & Ag_{10}…DBC, the electrostatic forces dominate and $\lambda_2\rho$ value shifted from −0.03 to −0.02 a. u. The appearance of green spike specifies the contribution from van der Waals dispersive interactions towards the stability of these composites. NCI study about the silver cluster-DBC composites show that there are sophisticated noncovalent interactions including electrostatic interactions, van der Waals dispersion and steric repulsion as indicated by NCI-RDG approach.

3.3. Frontier molecular orbitals analysis (FMO) of most stable Ag_n…DBC (n = 2–10) composites

In this section, the discussion of electronic properties is limited to the most stable structures for each cluster number over the surface of DBC. The interaction between silver clusters and DBC is described through the theory of frontier molecular orbital (FMO). The interactions of the highest occupied molecular orbital (HOMO) with the lowest unoccupied molecular orbital (LUMO) is related to the frontier molecular orbital analysis. The energies of the HOMO and LUMO are helpful in providing the information about the ionization potential (IP), electron affinity (EA) and HOMO-LUMO (H-L) gap besides

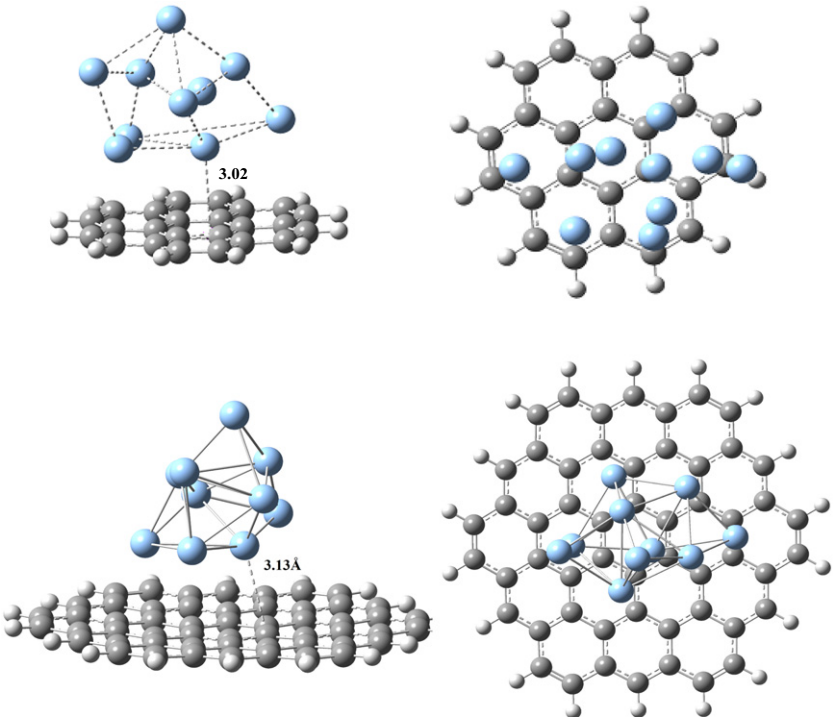

Fig. 7. Top view (R) and side view (L) of Ag_{10}…DBC (bottom) optimized at M06-2X-D3/LANL2DZ and Ag_{10}…Coronene (top) composites optimized at M06-2X/LANL2DZ.

predicting the reactivity and stability of a system [57]. The H-L gap for DBC is 4.35 eV which decreases to 3.34 eV when silver dimer is adsorbed on it (perpendicular orientation). The H-L gap further decreases to 2.98 eV for Ag_3…DBC complex. The H-L gap is quite low for Ag_4…DBC complex (2.48 eV) but it increases again in the case of Ag_5…DBC & Ag_6…DBC complexes to 2.62 & 3.23 eV, respectively. The H-L gap does not follow any regular pattern with the increasing number of silver atoms in the composite. The H-L gap first decreases from Ag_2 to Ag_4 in a regular manner but there is an increase in H-L gap from Ag_5 to Ag_6 silver cluster decorated DBC composites. The H-L gap in case of Ag_7…DBC is 2.43 eV, which is lower than that of Ag_6 decorated DBC. This decrease in H-L gap is due to increase in energy of HOMO and decrease in energy of LUMO. The H-L gap then increases to 2.89 eV for Ag_8…DBC, then falls onward in a regular way from Ag_9 to Ag_{10} silver cluster decorated DBC composites. The H-L gap for Ag_9…DBC & Ag_{10}…DBC composites are 2.37 & 2.16 eV, respectively. The H-L gap in case of Ag_{10} silver cluster decorated DBC complex is least amongst all studied silver clusters. One may argue that the HOMO-LUMO gap decreases when the number of silver atoms interacting with the DBC ring increase but to a maximum of four atoms on DBC. The H-L gap decreases again if the number of silver atoms interacting with DBC is greater than 4. For example, both Ag_3…DBC and Ag_8…DBC have three silver atoms interacting with DBC and they have the comparable H-L gap. The Ag_5…DBC and Ag_6…DBC have 5 and 6 six silver atoms and their H-L gaps are getting higher. Overall, the H-L gap are reduced for the silver cluster decorated DBC composites in comparison with DBC ring. The results of H-L gap show that there is a reasonable decrease H-L gap in Ag_n…DBC (n = 2–10) composites which certainly increase the conductivity of a system [72]. Analysis of the densities of HOMO and LUMO orbitals reveal that there are four distinct patterns for the distribution of densities (see Fig. 9). For Ag_2…DBC, the density of HOMO resides on DBC whereas LUMO is spread on both DBC and silver cluster. For Ag_3, Ag_4, Ag_7 & Ag_9 silver cluster decorated DBC composites, the density of HOMO reside on both DBC and metal cluster part while that of LUMO purely over silver clusters. However for Ag_8…DBC complex, the density of HOMO purely resides over silver cluster but LUMO partially over both silver cluster & DBC. The densities of both HOMO and LUMO for Ag_5, Ag_6 & Ag_{10} cluster decorated DBC are residing only on the metal center. This clearly illustrates that the HOMO energy levels of transition metal (Ag) are higher in energy than DBC. When combined, the silver atoms lead to the generation of new states between original HOMO and LUMO of DBC.

3.4. Ionization potentials and electron affinities of most stable Ag_n…DBC (n = 2–10) composites

According to Koopmann's theorem, the negative of HOMO is ionization potential (IP) whereas the negative of LUMO is electron affinity (EA). The HOMO can donate electrons whereas the LUMO has the ability to accept electrons. The value of IP for isolated DBC is 6.12 eV which decreases in a regular way to 5.23, 4.85 & 4.37 eV in Ag_2…DBC, Ag_3…DBC & Ag_4…DBC composites, respectively. This decrease in the value of IP is due to the increase in energy of occupied orbitals under the influence of electron-donating ability of silver clusters to DBC. An oscillating trend in the values of IP is observed in case of silver cluster decorated DBC composites (see Fig. 10). The Ag_2…DBC show the highest IP value whereas Ag_{10}…DBC has the lowest among all studied silver cluster decorated DBC composites. The lower value of IP, facilitates the electron transfer from silver to DBC ring. The ionization potentials of Ag_4, Ag_7 and, Ag_9 clusters decorated DBC are quite comparable to each other. There is also a quite regular osciallating trend in the values of electron affinities found for Ag_n…DBC composites. The value of electron affinity is the ability to accept electrons.

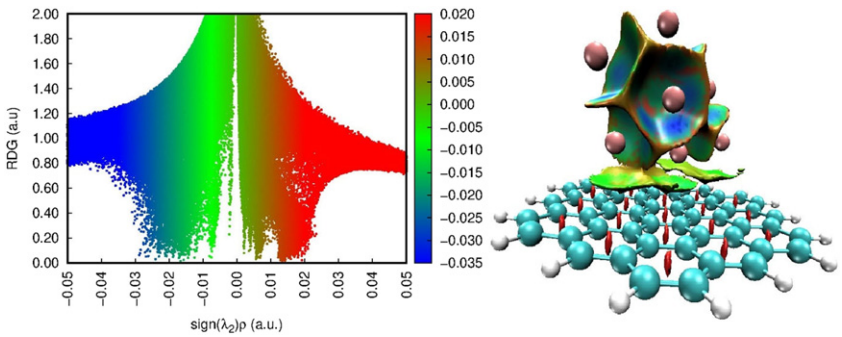

Fig. 8. NCI-RDG 2D scatter map (left) and 3D color-filled RDG isosurface (right) for Ag_{10}…DBC.

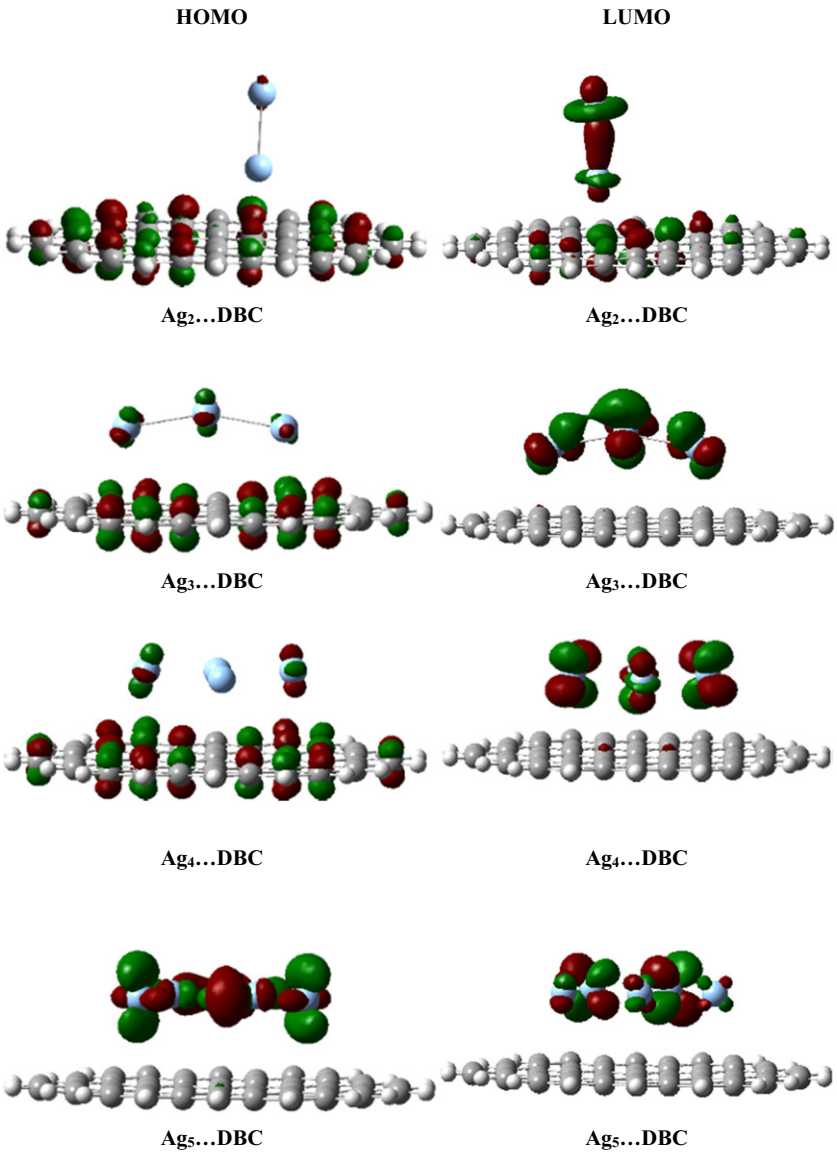

Fig. 9. HOMO-LUMO orbitals (top view) of most stable Ag_n…DBC (n = 2–10) composite system.

The Ag_3…DBC composite show the lowest EA of 1.86 eV whereas Ag_{10}…DBC has 2.04 eV, which is the highest in all studied silver cluster-DBC composites. The results of IP & EA, clearly show that the silver cluster decorated DBC composite system has the improved electron donating but poor electron accepting abilities as compared to pristine dodecabenzocoronene.

3.5. Chemical hardness (η) of the most stable Ag_n…DBC (n = 2-10) composites

The chemical hardness of the most stable Ag_n…DBC (n = 2–10) composites is calculated through equation (2) by using the values of VIP and EA. Chemical hardness is an electronic property used to describe the chemical stability of molecules and aggregates (Table 5). We employ chemical hardness here to define the stability and reactivity of our most stable Ag_n…DBC composites (n = 2–10) by the application of the principle of maximum hardness PMH explained by Pearson [72]. The chemical hardness of most stable Ag_n…DBC composites (n = 2–10) composites is illustrated in. The value of chemical hardness for Ag_2…DBC composite is 1.67 eV which keeps on decreasing up to Ag_{10}…DBC composite. The Ag_{10}…DBC has the least value of 1.08 eV among all Ag_n…DBC (n = 2–10) complexes studied.

There is a regular decrease in the value of chemical hardness up to Ag_4…DBC. The value for Ag_4…DBC is 1.24 eV but in case of Ag_5…DBC and Ag_6…DBC, the values of their chemical hardness are slightly increased to 1.31 and 1.61 eV, respectively. The value of chemical hardness of Ag_7…DBC is 1.21eV, which is lower than subsequent Ag_8…DBC composite (1.44 eV). The oscillating pattern in the values of chemical hardness might be due to the interaction of the different number of silver atoms at various top sites on DBC. The decreasing trend in the values of chemical hardness from Ag_2…DBC to Ag_{10}…DBC is due to the more efficient adsorption of silver clusters over DBC. The values of the chemical hardness of most stable Ag_n…DBC (n = 2–10) composites systems decrease in general as the number of silver atoms in the silver clusters increases. The Ag_2…DBC show the higest whereas the Ag_{10}…DBC has the lowest value of chemical hardness. It is clear from the trend in values of chemical hardness that the reactivity of Ag_n…DBC (n = 2–10) composites increases as the number of silver atoms in the clusters increases [57].

3.6. Softness (**S**) of most stable Ag_n…DBC (n = 2-10) composites

The softness values of the most stable Ag_n…DBC (n = 2–10) adsorbed systems can be calculated through equation (3) by using the values of vertical ionization potential (VIP) and electron affinity E.A. The softness of most stable Ag_n…DBC (n = 2–10) adsorbed systems are illustrated in Table 5. Softness value for Ag_2…DBC composite is 0.29 eV which is the least among all silver clusters decorated DBC composites studied. The value of softness increases in a regular pattern up to Ag_4…DBC composite, which has the value of 0.40 eV. The values of softness for Ag_5…DBC and Ag_6…DBC are 0.38 and 0.30 eV, respectively which suggest the greater stability of these composites than Ag_4…DBC. From Ag_7…DBC onwards the values of softness increase in a regular pattern except for Ag_8…DBC which has a low value of 0.34 eV.

It is also evident from the investigation that Ag_{10}…DBC has the higest value of softness (0.46 eV) and these composite systems are less stable among all Ag_n…DBC (n = 2–10) composites studied. There is a regular oscillating trend in the values of softness from Ag_2 to Ag_8 silver cluster decorated DBC, which might be due to the different number of silver atoms interacting with various top sites over DBC. In general, an increasing trend in the values of the softness of most stable Ag_n…DBC (n = 2–10) composites systems is

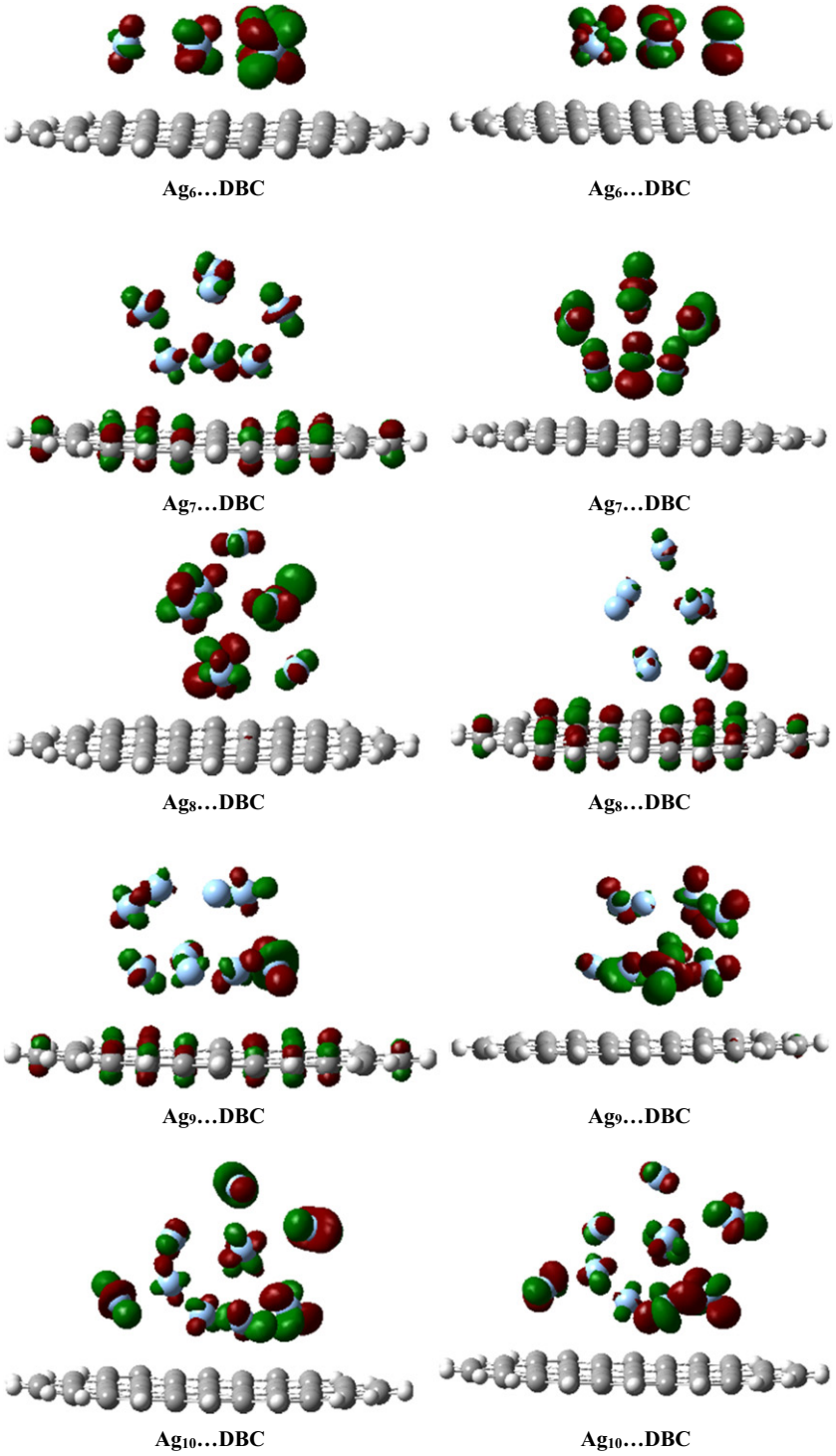

Fig. 9 (*continued*).

observed as compared to DBC. The values of softness suggested that the stability decreases from Ag_2…DBC to Ag_{10}…DBC composites. The reactivity of Ag_n…DBC (n = 2–10) increases as the number of silver atoms in the silver clusters increases. The overall increasing trend in the values of softness from Ag_2 to Ag_{10} silver cluster based DBC complosites is due to the more efficient adsorption of silver clusters over DBC.

3.7. Chemical potential (μ) of most stable Ag_n…DBC (n = 2-10) composite

The values for the chemical potential of most stable Ag_n-DBC (n = 2–10) composites are calculated from the values of highest occupied molecular orbital (HOMO) and lowest unoccupied molecular orbital (LUMO) by using equation (5). The values for the chemical potential of most stable Ag_n…DBC (n = 2–10) adsorbed systems are tabulated in Table 5. The value of chemical potential for isolated DBC is −3.94 eV which is increased to −3.56 eV in case of Ag_2…DBC composites. In the case of Ag_3…DBC & Ag_4…DBC the values of chemical potential are further increased to −3.35 & −3.13 eV, respectively. The values of chemical potential for Ag_n…DBC (n = 5 & 6) are −3.19 and −3.51 eV, respectively. In the case of Ag_7…DBC composite the value of chemical potential is same as that of Ag_4…DBC. There is a slight irregular decrease in the value of −3.43 eV is observed in case of Ag_8…DBC composite. After Ag_8…DBC the values of chemical potential increased in a regular pattern up to Ag_{10}…DBC. The overall increasing trend in the values of chemical potential for Ag_n…DBC composites show their high reactivity as compared to isolated DBC. Moreover, the results of chemical potential clearly indicates that the reactivity of Ag_n…

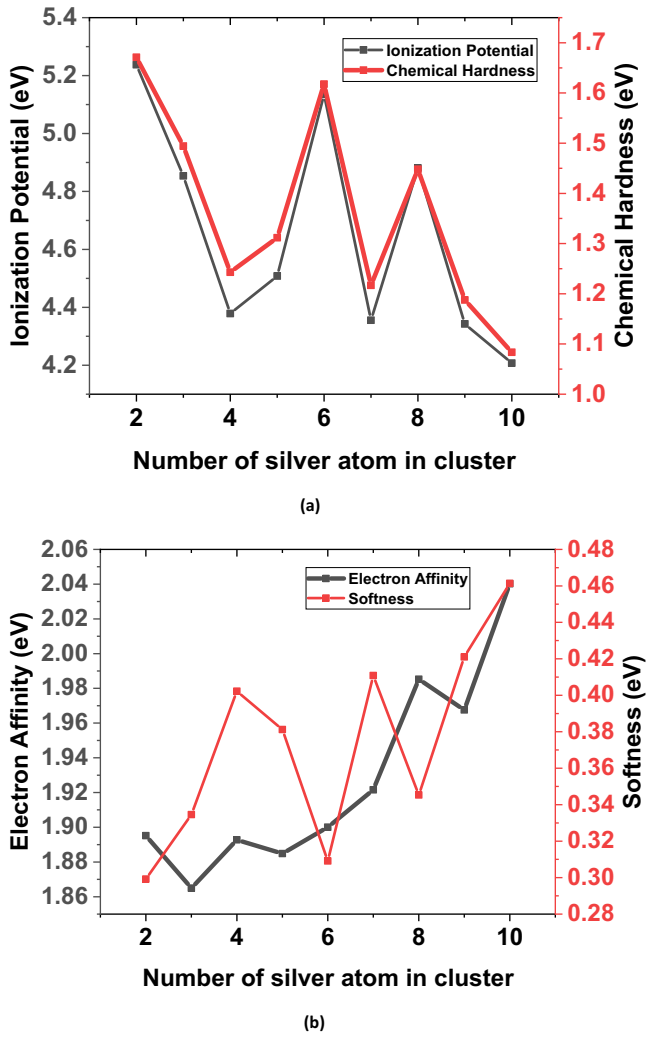

Fig. 10. Ionization potential & Chemical Hardness **(a)** Electron Affinity & Softness **(b)** of most stable Ag_n…DBC (n = 2–10) composites.

DBC composites also increased as the number of interacting silver atoms with DBC surface increases [57].

3.8. Fermi level (E_{FL}) of most stable Ag_n…DBC (n = 2-10) composites

The electrochemical potential for electrons is called Fermi level which is a thermodynamic quantity. The Fermi level can be explained by using the electronic band structure and determine the electronic properties of the system. The location of the Fermi level relative to the band energy levels is a critical feature in defining electronic properties. The values of the Fermi level for the most Ag_n…DBC (n = 2–10) adsorbed system is calculated by using equation (6). The values of the Fermi level for the most stable Ag_n…DBC (n = 2–10) adsorbed systems are shown in Table 4. The value of Fermi level for Ag_2…DBC composite is −3.56 eV which is increased to −3.35 eV in case of Ag_3…DBC composite. The higher value in case of Ag_3…DBC as compared to Ag_2…DBC, show its less stability. The Fermi level for Ag_2…DBC composite is the lowest among all Ag_n…DBC composites studied. The highest value of −3.12 eV is observed in case of Ag_{10}…DBC composite which reflects its least stability among Ag_n…DBC (n = 2–10) composites studied. The higher values of Fermi levels are observed in Ag_n…DBC when there are present an odd number of silver atoms in the cluster. The Ag_n…DBC composites comprising an even number of silver atoms in the cluster have lower values of Fermi levels [73].

Table 6
Charge Decomposition Analysis (CDA) results calculated at M062X-D3/LANL2DZ.

Composite	Donation	Backdonation	d-b	Repulsion
Ag_2… DBC	1.135	0.306	0.829	1.559
Ag_3… DBC	0.726	0.667	0.058	1.122
Ag_4… DBC	0.216	0.981	−0.764	0.351
Ag_5… DBC	−0.094	0.669	−0.764	0.358
Ag_6… DBC	−0.004	0.598	−0.603	−0.503
Ag_7… DBC	0.100	0.650	−0.550	0.455
Ag_8… DBC	0.547	−0.632	1.180	0.357
Ag_9… DBC	1.326	−0.233	1.559	−0.067
Ag_{10}… DBC	0.813	−0.845	1.659	1.181

3.9. Charge decomposition analysis (CDA)

Charge decomposition analysis (CDA) is unravelling scheme used to analyze the donor-acceptor interactions. CDA is a valuable method for evaluating the relative strength of charge donation and back-donation in complexes. CDA analysis is carried out to investigate the charge transfer between silver and DBC ring and the data are summarized in Table 6. We present here the results of CDA analysis to show the charge transfer interactions between various fragments, and we focus on the relative amount of forward donation and repulsion in the composite. CDA results revealed that charge donation and backdonation take place between d and π orbitals of silver and carbon of DBC, respectively. The amount of 0.829 ***e***, relative charge donation is observed in case of Ag_2…DBC composite. The amount of forward charge donation into d-orbitals of silver dimer is greater than π-back donation into orbitals of carbon in DBC. Quite similar trend of relative charge donation is found for Ag_3, Ag_8, Ag_9 & Ag_{10} silver cluster decorated DBC composites as we seen in case of Ag_2…DBC. The values of relative charge donation between silver clusters (Ag_3, Ag_8, Ag_9 & Ag_{10}) are 0.058, 1.180, 1.559 & 1.659 ***e*** , respectively. The extent of forward donation of charge into d-orbital of silver is more than π-back donation in these composites.

The highest amount of relative donation of charge observed in case of Ag_{10}…DBC composite, validate the strong overlap between π orbital of carbon with d-orbital of silver.

The amount of relative charge donation found for Ag_4, Ag_5, Ag_6 & Ag_7 silver cluster decorated DBC composites are −0.7645, −0.7642, −0.603 & −0.550 ***e***, respectively. The extent of π-back donation is more pronounced than forward donation into d-orbital in these silver cluster decorated DBC composites. The repulsion of charges is important indicator for charge density between donor and acceptor fragments. Generally, negative and positive values of repulsion correspond to moving away or accumulation of charge in interaction region. The values of repulsion of charges observed between the fragments of composite in Ag_2, Ag_3, Ag_4, Ag_5, Ag_7, Ag_8 & Ag_{10} silver clusters decorated DBC are 1.55, 1.12, 0.35, 0.35, 0.45, 0.35 & 1.18 ***e***, respectively. The values of repulsion are positive which suggest that charge is accumulated in interaction region between silver clusters and DBC. The value of repulsion observed in case of Ag_6 & Ag_9 are −0.50 & −0.06 ***e***, respectively. These values of repulsion of charges suggest that charge is moving away from bonding region between silver cluster and DBC fragments.

Table 5
Ionization potential, electron affinity, energies of highest occupied molecular orbital (HOMO), energies of lowest unoccupied molecular orbital (LUMO) and HOMO-LUMO gap, Chemical hardness (η), softness (S), chemical potential (μ) and Fermi level of most stable Ag_n…DBC (n = 2–10) composites calculated at M062X-D3/LANL2DZ. (Energies are calculated in the unit of eV).

System	I.P	E.A	E_H	E_L	H-L gap	η	S	μ	Fermi level
DBC	6.12	1.77	−6.12	−1.77	4.35	2.17	0.22	−3.94	−3.94
Ag_2… DBC	5.23	1.89	−5.23	−1.89	3.34	1.67	0.29	−3.56	−3.56
Ag_3… DBC	4.85	1.86	−4.85	−1.86	2.98	1.49	0.33	−3.35	−3.35
Ag_4… DBC	4.37	1.89	−4.37	−1.89	2.48	1.24	0.40	−3.13	−3.13
Ag_5… DBC	4.50	1.88	−4.50	−1.88	2.62	1.31	0.38	−3.19	−3.19
Ag_6… DBC	5.13	1.90	−5.13	−1.90	3.23	1.61	0.30	−3.51	−3.51
Ag_7… DBC	4.35	1.92	−4.35	−1.92	2.43	1.21	0.41	−3.13	−3.13
Ag_8… DBC	4.88	1.98	−4.88	−1.98	2.89	1.44	0.34	−3.43	−3.43
Ag_9… DBC	4.34	1.96	−4.34	−1.96	2.37	1.18	0.42	−3.15	−3.15
Ag_{10}… DBC	4.20	2.04	−4.20	−2.04	2.16	1.08	0.46	−3.12	−3.12

Table 7
ALMO-EDA results for several Ag_n…DBC complexes at the ω B97M-V/def2-SVPD/def2-ECP level with counterpoise-correction for CT energies. Results in kcal/mol.

System	E_{FRZ}	E_{POL}	E_{CT}	E_{int}
Ag_2-DBC	−3.074	−3.552	−2.942	−9.568
Ag_3-DBC	−8.213	−3.042	−2.513	−13.768
Ag_4-DBC	−10.676	−0.640	−0.876	−12.192
Ag_6-DBC	−17.638	−2.828	−3.419	−23.886
Ag_8-DBC	−12.642	−4.659	−3.660	−20.961
Ag_9-DBC	−17.672	−3.895	−3.765	−25.333
Ag_{10}-DBC	−15.764	−6.215	−4.786	−26.765

Table 8
CDFT charge-transfer analysis for Ag_n…DBC complexes at the ω B97M-V/def2-SVPD/def2-ECP level.

System	E_{CT} (kcal/mol)	Number of e^- (a.u.)	Direction of CT
Ag_2-DBC	−8.474	0.08	DBC-to-Ag
Ag_3-DBC	−8.429	0.06	DBC-to-Ag
Ag_4-DBC	−5.790	0.01	DBC-to-Ag
Ag_5-DBC	−7.810	0.04	DBC-to-Ag
Ag_6-DBC	−7.651	0.04	DBC-to-Ag
Ag_7-DBC	−8.891	0.10	DBC-to-Ag
Ag_8-DBC	−10.233	0.10	DBC-to-Ag
Ag_9-DBC	−11.949	0.11	DBC-to-Ag
Ag_{10}-DBC	−9.508	0.10	DBC-to-Ag

3.10. Energy decomposition analysis/charge transfer (EDA/CT)

The ALMO-EDA results for several of the Ag_n-DBC complexes are shown in Table 7. In general, the total interaction energy increases with silver cluster size. The extensivity of the interaction energy might be expected, given that London dispersion is likely to be dominant in these systems and dispersion is extensive with respect to number of electrons. This hypothesis is also supported by the fact that the frozen density energy becomes more attractive with silver cluster size. The contributions of polarization and CT show qualitative similarity in terms of relative magnitude with respect to silver cluster size. The clusters Ag_2–Ag_4 show a significant decrease in CT energy, while clusters Ag_6–Ag_{10} exhibit monotonic increase in CT energy. While the overall CT contribution becomes small with respect to the frozen density energy in larger clusters, it is certainly not insignificant at ~ 18% of the total interaction energy in Ag_{10}-DBC.

The CT analysis performed with CDFT was also used to assess not only the CT energy, but the number of electrons transferred. The CDFT CT energies shown in Table 8 are significantly larger than those obtained by ALMO-EDA, but they follow the same general qualitative trends. It is likely that the difference between the two methods in the predicted CT magnitude arises from the fact that the polarization/CT separation in the ALMO-EDA relies on a somewhat arbitrary truncation of the polarization response, where the CDFT method allows for infinite-order polarization. Like ALMO-EDA, CDFT predicts a sharp decrease in the CT energy in the clusters Ag_2–Ag_4, with larger CT predicted in clusters Ag_5–Ag_{10}. The predicted number of electrons transferred follows the same trend as the energy, with a maximum of about 0.1 electrons transferred in the largest silver clusters studied. In all cases, CDFT predicts CT from DBC to the silver cluster. When paired with the results for CT energy and number of electrons transferred, the direction of CT suggests that backdonation from DBC becomes dominant after the silver cluster reaches 5 atoms in size, displaying some agreement with the CDD results.

4. Summary

Graphene, a single atom thick two-dimensional sheet of sp^2 bonded carbon atom, has got remarkable interest due to its unique electronic structure. Spin-polarized DFT study of Ag_n…coronene (n = 2–10) systems reveals that these composites are stable in lower spin states. The interaction energy of Ag_2 for perpendicular orientation is higher than that of parallel orientations. For other clusters, the planar orientations on coronene possess higher interaction energies than perpendicular orientation mainly because of the higher number of interactions with coronene in planar orientation. Despite high interaction energies, many of the coplanar structures are not the lowest energies structures. CDA analysis reveals that backdonation from dodecabenzocoronene to silver clusters is more dominant in Ag_4–Ag_7 whereas other cluster have dominant charge transfer to dodecabenzocoronene. The EDA/CT analyses revealed that the larger silver clusters are likely bound to dodecabenzocoronene primarily by dispersive interactions, but charge-transfer from DBC to the silver clusters is non-negligible in its contribution to the total interaction energy at 18% of the interaction even in the largest system studied. NCI results also support the presence of van der Waals and electrostatic interactions. Most of the electronic properties show an oscillating behavior when plotted against the number of silver atoms in the cluster. The HOMO-LUMO gap is dependent on the number of interacting silver atoms with the coronene. The lowest values of H-L gaps are found where favorable interaction exists between coronene and silver clusters (Ag_4 and Ag_{10}), as revealed from the presence of densities on both fragments. The outcome of the present study is the improved electronic properties, which may provide valuable insight and useful guideline for the development and various applications of silver cluster-based graphene composites.

Acknowledgments

The authors acknowledge financial and technical support from COMSATS University, Abbottabad Campus and Higher Education Commission of Pakistan (Grant # 1899, 2469, 2981). Work by K.C.-F. and J.M.H. was supported by the U.S. Department of Energy, Office of Basic Energy Sciences, Division of Chemical Sciences, Geosciences, and Biosciences under Award No. DE-SC0008550.

Appendix A. Supplementary data

Supplementary data to this article can be found online at https://doi.org/10.1016/j.molliq.2019.111902.

References

[1] M. Pumera, A. Ambrosi, A. Bonanni, E.L.K. Chng, H.L. Poh, Graphene for electrochemical sensing and biosensing, TrAC Trends Anal. Chem. (Reference Ed.) 29 (2010) 954–965, https://doi.org/10.1016/j.trac.2010.05.011.
[2] G. Ning, Z. Fan, G. Wang, J. Gao, W. Qian, F. Wei, Gram-scale synthesis of nanomesh graphene with high surface area and its application in supercapacitor electrodes, Chem. Commun. 47 (2011) 5976, https://doi.org/10.1039/c1cc11159k.
[3] Z.-S. Wu, W. Ren, L. Gao, J. Zhao, Z. Chen, B. Liu, D. Tang, B. Yu, C. Jiang, H.-M. Cheng, Synthesis of graphene sheets with high electrical conductivity and good thermal stability by hydrogen arc discharge exfoliation, ACS Nano 3 (2009) 411–417, https://doi.org/10.1021/nn900020u.
[4] A.H. Castro Neto, F. Guinea, N.M.R. Peres, K.S. Novoselov, A.K. Geim, The electronic properties of graphene, Rev. Mod. Phys. 81 (2009) 109–162, https://doi.org/10.1103/RevModPhys.81.109.

[5] I.W. Frank, D.M. Tanenbaum, A.M. van der Zande, P.L. McEuen, Mechanical properties of suspended graphene sheets, J. Vac. Sci. Technol. B Microelectron. Nanom. Struct. 25 (2007) 2558, https://doi.org/10.1116/1.2789446.
[6] S. Tongay, K. Berke, M. Lemaitre, Z. Nasrollahi, D.B. Tanner, A.F. Hebard, B.R. Appleton, Stable hole doping of graphene for low electrical resistance and high optical transparency, Nanotechnology 22 (2011) 425701, https://doi.org/10.1088/0957-4484/22/42/425701.
[7] Y. Huang, J. Liang, Y. Chen, An overview of the applications of graphene-based materials in supercapacitors, Small 8 (2012) 1805–1834, https://doi.org/10.1002/smll.201102635.
[8] S. Zhang, L. Sui, H. Kang, H. Dong, L. Dong, L. Yu, High performance of N-doped graphene with bubble-like textures for supercapacitors, Small 14 (2018) 1702570, https://doi.org/10.1002/smll.201702570.
[9] L. Sui, Y. Wang, W. Ji, H. Kang, L. Dong, L. Yu, N-doped ordered mesoporous carbon/graphene composites with supercapacitor performances fabricated by evaporation induced self-assembly, Int. J. Hydrogen Energy 42 (2017) 29820–29829, https://doi.org/10.1016/j.ijhydene.2017.10.113.
[10] H. Wang, X. Yuan, Y. Wu, H. Huang, X. Peng, G. Zeng, H. Zhong, J. Liang, M. Ren, Graphene-based materials: fabrication, characterization and application for the decontamination of wastewater and wastegas and hydrogen storage/generation, Adv. Colloid Interface Sci. 195–196 (2013) 19–40, https://doi.org/10.1016/j.cis.2013.03.009.
[11] M. Pumera, Graphene-based nanomaterials for energy storage, Energy Environ. Sci. 4 (2011) 668–674, https://doi.org/10.1039/C0EE00295J.
[12] M. Liang, L. Zhi, Graphene-based electrode materials for rechargeable lithium batteries, J. Mater. Chem. 19 (2009) 5871, https://doi.org/10.1039/b901551e.
[13] P.T. Moseley, Solid state gas sensors, Meas. Sci. Technol. 8 (1997) 223–237, https://doi.org/10.1088/0957-0233/8/3/003.
[14] Y. Shao, J. Wang, H. Wu, J. Liu, I.A. Aksay, Y. Lin, Graphene based electrochemical sensors and biosensors: a review, Electroanalysis 22 (2010) 1027–1036, https://doi.org/10.1002/elan.200900571.
[15] B.F. Machado, P. Serp, Graphene-based materials for catalysis, Catal. Sci. Technol. 2 (2012) 54–75, https://doi.org/10.1039/C1CY00361E.
[16] S. Zhang, L. Sui, H. Dong, W. He, L. Dong, L. Yu, High-performance supercapacitor of graphene quantum dots with uniform sizes, ACS Appl. Mater. Interfaces 10 (2018) 12983–12991, https://doi.org/10.1021/acsami.8b00323.
[17] J. Yu, X. Gao, Z. Cui, Y. Jiao, Q. Zhang, H. Dong, L. Yu, L. Dong, Facile synthesis of binary transition metal sulfide tubes derived from NiCo-MOF-74 for high-performance supercapacitors, Energy Technol. 7 (2019) 1900018, https://doi.org/10.1002/ente.201900018.
[18] W.X. Wang, S.H. Liang, T. Yu, D.H. Li, Y.B. Li, X.F. Han, The study of interaction between graphene and metals by Raman spectroscopy, J. Appl. Phys. 109 (2011), 07C501. https://doi.org/10.1063/1.3536670.
[19] R.N. Lenz Baldez, P. Piquini, A.A. Schmidt, M.A. Kuroda, Tunable interaction between metal clusters and graphene, Phys. Chem. Chem. Phys. 19 (2017) 22153–22160, https://doi.org/10.1039/C7CP04615D.
[20] H. Liu, Y. Liu, D. Zhu, Chemical doping of graphene, J. Mater. Chem. 21 (2011) 3335–3345, https://doi.org/10.1039/C0JM02922J.
[21] H. Yin, H. Tang, D. Wang, Y. Gao, Z. Tang, Facile synthesis of surfactant-free Au cluster/graphene hybrids for high-performance oxygen reduction reaction, ACS Nano 6 (2012) 8288–8297, https://doi.org/10.1021/nn302984x.
[22] W. Song, J. Wang, B. Wang, W. Hu, Y. Wang, First-principles study on the structures and electronic properties of graphene-supported Ni n (n = 1–6) clusters, Mol. Simul. (2018) 1–10, https://doi.org/10.1080/08927022.2018.1517413.
[23] H. Song, X. Li, P. Cui, S. Guo, W. Liu, X. Wang, Morphology optimization of CVD graphene decorated with Ag nanoparticles as ammonia sensor, Sens. Actuators B Chem. 244 (2017) 124–130, https://doi.org/10.1016/j.snb.2016.12.133.
[24] D.-T. Phan, G.-S. Chung, A novel Pd nanocube–graphene hybrid for hydrogen detection, Sens. Actuators B Chem. 199 (2014) 354–360, https://doi.org/10.1016/j.snb.2014.04.013.
[25] W. Xue, X. Bo, M. Zhou, L. Guo, Enzymeless electrochemical detection of hydrogen peroxide at Pd nanoparticles/porous graphene, J. Electroanal. Chem. 781 (2016) 204–211, https://doi.org/10.1016/j.jelechem.2016.05.036.
[26] J. Wang, H. Sun, H. Pan, Y. Ding, J. Wan, G. Wang, M. Han, Detection of hydrogen peroxide at a palladium nanoparticle-bilayer graphene hybrid-modified electrode, Sens. Actuators B Chem. 230 (2016) 690–696, https://doi.org/10.1016/j.snb.2016.02.117.
[27] J. N'Diaye, S. Poorahong, O. Hmam, R. Izquierdo, M. Siaj, Facile synthesis rhodium nanoparticles decorated single layer graphene as an enhancement hydrogen peroxide sensor, J. Electroanal. Chem. 789 (2017) 85–91, https://doi.org/10.1016/j.jelechem.2017.01.061.
[28] M. Liu, W. Chen, Graphene nanosheets-supported Ag nanoparticles for ultrasensitive detection of TNT by surface-enhanced Raman spectroscopy, Biosens. Bioelectron. 46 (2013) 68–73, https://doi.org/10.1016/j.bios.2013.01.073.
[29] S. Nasresfahani, R. Safaiee, M.H. Sheikhi, Influence of Pd/Pd 2 decoration on the structural, electronic and sensing properties of monolayer graphene in the presence of methane molecule: a dispersion-corrected DFT study, Surf. Sci. 662 (2017) 93–101, https://doi.org/10.1016/j.susc.2017.04.002.
[30] S. Basu, S. Hazra, Graphene–noble metal nano-composites and applications for hydrogen sensors, Chimia 3 (2017) 29, https://doi.org/10.3390/c3040029.
[31] F. Schedin, A.K. Geim, S.V. Morozov, E.W. Hill, P. Blake, M.I. Katsnelson, K.S. Novoselov, Detection of individual gas molecules adsorbed on graphene, Nat. Mater. 6 (2007) 652–655, https://doi.org/10.1038/nmat1967.
[32] Z. Zhou, F. Gao, D.W. Goodman, Deposition of metal clusters on single-layer graphene/Ru(0001): factors that govern cluster growth, Surf. Sci. 604 (2010) L31–L38, https://doi.org/10.1016/j.susc.2010.03.008.
[33] E. Yoo, T. Okata, T. Akita, M. Kohyama, J. Nakamura, I. Honma, Enhanced electrocatalytic activity of Pt subnanoclusters on graphene nanosheet surface, Nano Lett. 9 (2009) 2255–2259, https://doi.org/10.1021/nl900397t.
[34] A.T. N'Diaye, S. Bleikamp, P.J. Feibelman, T. Michely, Two-dimensional Ir cluster lattice on a graphene moiré on Ir(111), Phys. Rev. Lett. 97 (2006) 215501, https://doi.org/10.1103/PhysRevLett.97.215501.
[35] H. Lee, J. Ihm, M.L. Cohen, S.G. Louie, Calcium-decorated graphene-based nanostructures for hydrogen storage, Nano Lett. 10 (2010) 793–798, https://doi.org/10.1021/nl902822s.
[36] Y.-H. Lu, M. Zhou, C. Zhang, Y.-P. Feng, Metal-embedded graphene: a possible catalyst with high activity, J. Phys. Chem. C 113 (2009) 20156–20160, https://doi.org/10.1021/jp908829m.
[37] D. Shahabi, H. Tavakol, A DFT study on the catalytic ability of aluminum doped graphene for the initial steps of the conversion of methanol to gasoline, Comput. Theor. Chem. 1127 (2018) 8–15, https://doi.org/10.1016/j.comptc.2018.02.001.
[38] Y. Zhang, X. Yuan, Y. Wang, Y. Chen, One-pot photochemical synthesis of graphene composites uniformly deposited with silver nanoparticles and their high catalytic activity towards the reduction of 2-nitroaniline, J. Mater. Chem. 22 (2012) 7245, https://doi.org/10.1039/c2jm16455h.
[39] K.M.F. Shahil, A.A. Balandin, Thermal properties of graphene and multilayer graphene: applications in thermal interface materials, Solid State Commun. 152 (2012) 1331–1340, https://doi.org/10.1016/j.ssc.2012.04.034.
[40] J. Li, C. Liu, Ag/Graphene heterostructures: synthesis, characterization and optical properties, Eur. J. Inorg. Chem. 2010 (2010) 1244–1248, https://doi.org/10.1002/ejic.200901048.
[41] D. Zhang, P. Wang, Y. Fang, The surface-enhanced Raman spectroscopy of graphene deposited by silver nanoparticle islands, Integr. Ferroelectr. 147 (2013) 90–96, https://doi.org/10.1080/10584587.2013.792207.
[42] A. Chandrasekar, T. Pradeep, Luminescent silver clusters with covalent functionalization of graphene, J. Phys. Chem. C 116 (2012) 14057–14061, https://doi.org/10.1021/jp304131v.
[43] K.S. Subrahmanyam, A.K. Manna, S.K. Pati, C.N.R. Rao, A study of graphene decorated with metal nanoparticles, Chem. Phys. Lett. 497 (2010) 70–75, https://doi.org/10.1016/j.cplett.2010.07.091.
[44] J. Granatier, P. Lazar, M. Otyepka, P. Hobza, The nature of the binding of Au, Ag, and Pd to benzene, coronene, and graphene: from benchmark CCSD(T) calculations to plane-wave DFT calculations, J. Chem. Theory Comput. 7 (2011) 3743–3755, https://doi.org/10.1021/ct200625h.
[45] Y. Zhao, D.G. Truhlar, Exploring the limit of accuracy of the global hybrid meta density functional for main-group thermochemistry, kinetics, and noncovalent interactions, J. Chem. Theory Comput. 4 (2008) 1849–1868, https://doi.org/10.1021/ct800246v.
[46] Y. Zhao, D.G. Truhlar, Density functionals for noncovalent interaction energies of biological importance, J. Chem. Theory Comput. 3 (2007) 289–300, https://doi.org/10.1021/ct6002719.
[47] Y. Zhao, D.G. Truhlar, The M06 suite of density functionals for main group thermochemistry, thermochemical kinetics, noncovalent interactions, excited states, and transition elements: two new functionals and systematic testing of four M06-class functionals and 12 other function, Theor. Chem. Acc. 120 (2008) 215–241, https://doi.org/10.1007/s00214-007-0310-x.
[48] T.-T. Jia, C.-H. Lu, K.-N. Ding, Y.-F. Zhang, W.-K. Chen, Oxidation of Pdn (n=1–5) clusters on single vacancy graphene: a first-principles study, Comput. Theor. Chem. 1020 (2013) 91–99, https://doi.org/10.1016/j.comptc.2013.07.029.
[49] T. Alonso-Lanza, Á. Mañanes, A. Ayuela, Interaction of cobalt atoms, dimers, and Co 4 clusters with circumcoronene: a theoretical study, J. Phys. Chem. C 121 (2017) 18900–18908, https://doi.org/10.1021/acs.jpcc.7b04369.
[50] H. Johll, H.C. Kang, E.S. Tok, Density functional theory study of Fe, Co, and Ni adatoms and dimers adsorbed on graphene, Phys. Rev. B. 79 (2009) 245416, https://doi.org/10.1103/PhysRevB.79.245416.
[51] C. Cao, M. Wu, J. Jiang, H.-P. Cheng, Transition metal adatom and dimer adsorbed on graphene: induced magnetization and electronic structures, Phys. Rev. B. 81 (2010) 205424, https://doi.org/10.1103/PhysRevB.81.205424.
[52] I. Khan, J. Hong, Magnetic properties of transition metal Mn, Fe and Co dimers on monolayer phosphorene, Nanotechnology 27 (2016) 385701, https://doi.org/10.1088/0957-4484/27/38/385701.
[53] T. Alonso-Lanza, A. Ayuela, F. Aguilera-Granja, Chemical bonding of transition-metal Co 13 clusters with graphene, ChemPhysChem 16 (2015) 3700–3710, https://doi.org/10.1002/cphc.201500692.
[54] Y. Mao, J. Yuan, J. Zhong, Density functional calculation of transition metal adatom adsorption on graphene, J. Phys. Condens. Matter 20 (2008) 115209, https://doi.org/10.1088/0953-8984/20/11/115209.
[55] T.O. Wehling, A.I. Lichtenstein, M.I. Katsnelson, Transition-metal adatoms on graphene: influence of local Coulomb interactions on chemical bonding and magnetic moments, Phys. Rev. B. 84 (2011) 235110, https://doi.org/10.1103/PhysRevB.84.235110.
[56] I. Cabria, M.J. López, J.A. Alonso, Theoretical study of the transition from planar to three-dimensional structures of palladium clusters supported on graphene, Phys. Rev. B. 81 (2010), 035403. https://doi.org/10.1103/PhysRevB.81.035403.
[57] M. Amft, B. Sanyal, O. Eriksson, N. V Skorodumova, Small gold clusters on graphene, their mobility and clustering: a DFT study, J. Phys. Condens. Matter 23 (2011) 205301, https://doi.org/10.1088/0953-8984/23/20/205301.
[58] K. Okazaki-Maeda, Y. Morikawa, S. Tanaka, M. Kohyama, Structures of Pt clusters on graphene by first-principles calculations, Surf. Sci. 604 (2010) 144–154, https://doi.org/10.1016/j.susc.2009.11.001.
[59] R.C. Longo, J. Carrete, L.J. Gallego, Ab initio study of 3 d , 4 d , and 5 d transition metal adatoms and dimers adsorbed on hydrogen-passivated zigzag graphene

nanoribbons, Phys. Rev. B. 83 (2011) 235415, https://doi.org/10.1103/PhysRevB.83.235415.
[60] X. Xing, A. Hermann, X. Kuang, M. Ju, C. Lu, Y. Jin, X. Xia, G. Maroulis, Insights into the geometries, electronic and magnetic properties of neutral and charged palladium clusters, Sci. Rep. 6 (2016) 19656, https://doi.org/10.1038/srep19656.
[61] B. Zhan, C. Liu, H. Shi, C. Li, L. Wang, W. Huang, X. Dong, A hydrogen peroxide electrochemical sensor based on silver nanoparticles decorated three-dimensional graphene, Appl. Phys. Lett. 104 (2014) 243704, https://doi.org/10.1063/1.4884418.
[62] X. Liu, C.-Z. Wang, H.-Q. Lin, M. Hupalo, P.A. Thiel, K.-M. Ho, M.C. Tringides, Structures and magnetic properties of Fe clusters on graphene, Phys. Rev. B. 90 (2014) 155444, https://doi.org/10.1103/PhysRevB.90.155444.
[63] M.J. Frisch, G.W. Trucks, H.B. Schlegel, G.E. Scuseria, M.A. Robb, J.R. Cheeseman, G. Scalmani, V. Barone, G.A. Petersson, H. Nakatsuji, X. Li, M. Caricato, A. Marenich, J. Blonio, B.G. Janesko, R. Gomperts, B. Mennucci, H.P. Hratchian, J.V. Ortiz, A.F. Izmaylov, J.L. Sonnenberg, D. Williams-Young, F. Ding, F. Lipparini, F. Egidi, J. Goings, B. Peng, A. Petrone, T. Henderson, D. Ranasinghe, V.G. Zakrzewski, J. Gao, N. Rega, G. Zheng, W. Liang, M. Hada, M. Ehara, K. Toyota, R. Fukuda, J. Hasegawa, M. Ishida, T. Nakajima, Y. Honda, O. Kitao, H. Nakai, T. Vreven, K. Throssell, J.A. Montgomery Jr., J.E. Peralta, F. Ogliaro, M. Bearpark, J.J. Heyd, E. Brothers, K.N. Kudin, V.N. Staroverov, T. Keith, R. Kobayashi, J. Normand, K. Raghavachari, A. Rendell, J.C. Burant, S.S. Iyengar, J. Tomasi, M. Cossi, J.M. Millam, M. Klene, C. Adamo, R. Cammi, J.W. Ochterski, R.L. Martin, K. Morokuma, O. Farkas, J.B. Foresman, J.B. Foresman, D.J. Fox, Gaussian, Inc., Wallingford CT, 2016 (n.d.).
[64] S. Grimme, J. Antony, S. Ehrlich, H. Krieg, A consistent and accurate ab initio parametrization of density functional dispersion correction (DFT-D) for the 94 elements H-Pu, J. Chem. Phys. 132 (2010) 154104, https://doi.org/10.1063/1.3382344.
[65] H. Ullah, A.-H.A. Shah, S. Bilal, K. Ayub, DFT study of polyaniline NH 3 , CO 2 , and CO gas sensors: comparison with recent experimental data, J. Phys. Chem. C 117 (2013) 23701–23711, https://doi.org/10.1021/jp407132c.
[66] H. Ullah, K. Ayub, Z. Ullah, M. Hanif, R. Nawaz, A.-H.A. Shah, S. Bilal, Theoretical insight of polypyrrole ammonia gas sensor, Synth. Met. 172 (2013) 14–20, https://doi.org/10.1016/j.synthmet.2013.03.021.
[67] F. Wasim, T. Mahmood, K. Ayub, An accurate cost effective DFT approach to study the sensing behaviour of polypyrrole towards nitrate ions in gas and aqueous phases, Phys. Chem. Chem. Phys. 18 (2016) 19236–19247, https://doi.org/10.1039/C6CP02271E.
[68] P.R. Horn, Y. Mao, M. Head-Gordon, Probing non-covalent interactions with a second generation energy decomposition analysis using absolutely localized molecular orbitals, Phys. Chem. Chem. Phys. 18 (2016) 23067–23079, https://doi.org/10.1039/C6CP03784D.
[69] K.U. Lao, J.M. Herbert, Energy decomposition analysis with a stable charge-transfer term for interpreting intermolecular interactions, J. Chem. Theory Comput. 12 (2016) 2569–2582, https://doi.org/10.1021/acs.jctc.6b00155.
[70] N. Mardirossian, M. Head-Gordon, ω B97M-V: a combinatorially optimized, range-separated hybrid, meta-GGA density functional with VV10 nonlocal correlation, J. Chem. Phys. 144 (2016) 214110, https://doi.org/10.1063/1.4952647.
[71] N. Mardirossian, M. Head-Gordon, Thirty years of density functional theory in computational chemistry: an overview and extensive assessment of 200 density functionals, Mol. Phys. 115 (2017) 2315–2372, https://doi.org/10.1080/00268976.2017.1333644.
[72] M.V. Putz, in: D.M.P. Mingos (Ed.), Applications of Density Functional Theory to Chemical Reactivity, Springer Berlin Heidelberg, Berlin, Heidelberg, 2012https://doi.org/10.1007/978-3-642-32753-7.
[73] R. Hussain, A.I. Hussain, S.A.S. Chatha, R. Hussain, U. Hanif, K. Ayub, Density functional theory and surface reactivity study of bimetallic Ag n Y m (n+m = 10) clusters, Solid State Sci. 80 (2018) 46–64, https://doi.org/10.1016/j.solidstatesciences.2018.03.015.